e-ISSN: 3061-9629

2 cilt volume
1 sayı issue
2025 Ocak january

HITIT JOURNAL OF SCIENCE

HİTİT ÜNİVERSİTESİ YAYINLARI

HİTİT JOURNAL OF SCIENCE

e-ISSN: 3061-9629
Volume: 2 • Issue: 1 - January 2025
Period: 2 Issues per Year (January & July)

LANGUAGE OF PUBLICATION
English

CONTACT ADDRESS
Hitit Üniversitesi Fen Edebiyat Fakültesi, ÇORUM, TÜRKİYE
Tel: +90 364 222 11 00 Fax: +90 364 222 11 02
hjs@hitit.edu.tr | https://dergipark.org.tr/tr/pub/hjs

PUBLISHER
Hitit University Press

HAKEM KURULU | REFEREE BOARD

Hitit Medical Journal Dergisi, çift taraflı kör hakemlik sistemi kullanmaktadır. Hakem isimleri gizli tutulmakta ve yayımlanmamaktadır.

Hitit Medical Journal uses a double-blind review. Referee names are kept strictly confidential.

LOCKSS: https://dergipark.org.tr/tr/pub/hjs/lockss-manifest

OAI: https://dergipark.org.tr/api/public/oai/hjs/

BOARD OF EDITORS

Editörden

Değerli Okuyucular;
Hitit Journal of Science 2025 yılının ilk sayısı ile sizlerle buluşmaktan büyük bir mutluluk duyuyoruz. Dergimize olan ilgi ve destek için teşekkür ederiz.
Dergimizde, Temel Bilimler (Fizik, Kimya, Biyoloji ve Matematik) alanında kapsamlı ve çeşitli makaleler yayımlamaya özen gösteriyoruz. Bu sayıda da bilim dünyasına katkı sağlayacak 2'si araştırma makalesi olmak üzere toplam 3 makaleyi siz değerli okuyucularımızla paylaşmanın gururunu yaşıyoruz.
Tüm okuyucularımıza keyifli ve verimli okumalar diliyoruz.
Saygılarımızla,

Prof. Dr. Dursun Ali KÖSE
HJS Editöryal Kurul adına

From the Editor

Dear Readers;

Hitit Journal of Science is very pleased to meet you with the first issue of 2025. Thank you for your interest and support for our journal. In our journal, we strive to publish comprehensive and diverse articles in the field of Basic Sciences (Physics, Chemistry, Biology, and Mathematics). In this issue, we take pride in sharing a total of 3 articles, including 2 research papers, with our esteemed readers, contributing to the world of science. We wish all our readers enjoyable and productive reading.
Regards,

Prof. Dr. Dursun Ali KÖSE
On behalf of the HJS Editorial Board

INDEX

HİTİT JOURNAL OF SCIENCE

e-ISSN: 3061-9629
Volume: 2 • Number: 1
January 2025

A Novel Review: Association of Alzheimer's Disease with the SUMO Protein Family

Beyza AYDIN

Department of Molecular Biology and Genetics, Karadeniz Tecnichal University, Trabzon, Türkiye.

Corresponding Author

Beyza AYDIN
E-mail: abeyza000@gmail.com Phone:
RORID: ror.org/03z8fyr40

Article Information

Article Type: Review
Doi: -
Received: 16.06.2024
Accepted: 17.11.2024
Published: 31.01.2025

Cite As

Aydın B. A Novel Review: Association of Alzheimer's Disease with the SUMO Protein Family. Hitit journal of Science. 2025;2(1):1-8.

Peer Review: Evaluated by independent reviewers working in at least two different institutions appointed by the field editor.
Ethical Statement: Not available.
Plagiarism Checks: Yes - iThenticate
Conflict of Interest: Authors approve that to the best of their knowledge, there is not any conflict of interest or common interest with an institution/ organization or a person that may affect the review process of the paper.

CRedit Author Statement
Beyza AYDIN: Design of the study, writing, reviewing, editing, supervisio

A Novel Review: Association of Alzheimer's Disease with the SUMO Protein Family

Beyza AYDIN*
Department of Molecular Biology and Genetics, Karadeniz Tecnichal University, Trabzon, Türkiye.

Abstract
Neurodegenerative diseases are conditions marked by the gradual deterioration and loss of neurons. In more advanced stages, this results in impairments in cognitive function and motor activity. These disorders may arise from a combination of internal and environmental causes, including genetic predisposition, the natural process of aging, dietary habits, and psychological stress. Multiple studies have shown that protein aggregation is a prevalent characteristic of neurodegenerative disorders. Misfolded or inadequately expressed proteins have a substantial influence on the advancement of many disorders. Recent investigations have shown that certain paralogs of SUMO proteins have a substantial impact on neurodegenerative disorders. This study specifically examines Alzheimer's disease, a well-known neurodegenerative disorder, and investigates the influence of SUMO proteins on the development and progression of this illness. Empirical evidence indicates that this group of proteins governs cellular processes by means of post-translational changes, exerting both beneficial and detrimental effects on Alzheimer's disease. Several factors contribute to Alzheimer's disease, a complex neurological ailment that causes brain function to degrade. It is becoming more common worldwide due to the rising number of elderly individuals. Examining the impact of SUMO proteins from this standpoint provides encouraging insights into future therapies for these now-untreatable conditions.

Keywords: Alzheimer's, Neurodegenerative, SUMO protein family, Apo-E4, Ubiquitin.

Introduction
Neurodegenerative diseases are characterized by the progressive loss of neurons, leading to the subsequent degeneration of specific brain regions and resulting in the loss of nervous system functions associated with this neuronal decline[1]. A common feature in the pathophysiology of these diseases is the aggregation of misfolded proteins [2]. The inability to maintain protein stability can arise due to the expression of mutated genes or post-translational modifications, leading to misfolding [3]. Therefore, post-translational modifications are crucial within the cell. Examples of neurodegenerative diseases include Dentatorubral-Pallidoluysian Atrophy, Spinobulbar Muscular Atrophy, Neuronal Intranuclear Inclusion Disease, Parkinson's Disease, Alzheimer's Disease, and Huntington's Disease [4]. In Alzheimer's disease, this review article will examine the role of the sumoylation cycle, a post-translational modification involving the attachment of SUMO (Small Ubiquitin-related modifier) proteins to lysine residues of target proteins. The sumoylation process often affects events involved in neurodegeneration, such as protein aggregation, mitochondrial dysfunction, oxidative stress, RNA transcription, and metabolism [5].

Protein Aggregation Mechanisms in Alzheimer's Disease
Alzheimer's Disease (AD) is characterized by the extracellular accumulation of amyloid plaques (Aβ plaques) and the intracellular aggregation of neurofibrillary tangles (NFTs) within the brain. The aggregation of Aβ plaques and NFTs is recognized as a hallmark of AD pathology, as these structures interfere with neuronal communication at synapses. In the amyloidogenic pathway, Aβ plaques is produced through the sequential cleavage of amyloid precursor protein (APP) by β-secretase and γ-secretase, whereas in the non-amyloidogenic pathway, α-secretase acts as the key enzyme, preventing Aβ formation [53]. In addition to Aβ, hyperphosphorylated tau proteins, resulting from the action of various kinases, lead to the formation of abnormal filamentous bundles, which are also present in the AD brain. Early-onset AD is associated with rare autosomal dominant mutations in three genes: APP, presenilin 1 (PSEN1), and presenilin 2 (PSEN2), while late-onset AD is strongly correlated with polymorphisms in the apolipoprotein E (APOE) gene. These mutations influence the production of Aβ peptides, a major component of senile plaques. Beyond APOE, other risk variants in genes such as ADAM10, ADAMTS1, MAPT, GRN, ARSA, and CSF1R are implicated in APP and tau metabolism in late-onset AD [54].

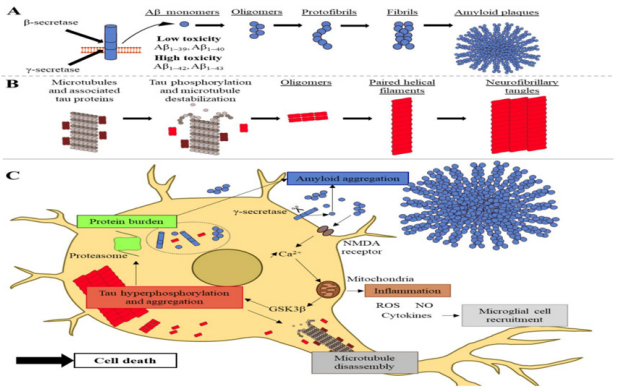

Figure1: Molecular Features of Alzheimer's Disease. (A) Production and Aggregation of Amyloid Peptides: The amyloid precursor protein (APP) is cleaved by β- and γ-secretases, forming Aβ peptides. These peptides aggregate into toxic oligomers, protofibrils, fibrils, and amyloid plaques under pathological conditions. (B) Tau Protein Aggregation: Tau proteins, normally associated with microtubules, become hyperphosphorylated during disease progression, dissociate, and aggregate into oligomers, paired helical filaments, and neurofibrillary tangles (NFTs). (C) Molecular Interactions in Neurons during AD and the Tau–Aβ Feedback Loop: Aβ oligomers increase calcium levels, triggering inflammation, microglial activation, and promoting tau aggregation. Hyperphosphorylated tau destabilizes microtubules, enhances tau aggregation, and interferes with Aβ degradation, contributing to neuronal death. Abbreviations: NMDA, N-methyl-D-aspartate; GSK3β, glycogen synthase kinase 3 beta; ROS, reactive oxygen species; NO, nitric oxide. (Vignon A., Salvador-Prince L. et al., Int. J. Mol. Sci. *2021)*[60]

As seen in Figure 1,the clearance of Aβ and tau proteins occurs through several mechanisms, including lysosomal degradation, ubiquitination and proteasomal degradation, microglial phagocytosis, and transport via interstitial fluid (ISF), the blood-brain barrier (BBB), and cerebrospinal fluid

(CSF). Two transmembrane receptors on endothelial cells, the lipoprotein receptor-related protein (LRP) and the receptor for advanced glycation end products (RAGE), are involved in the transport of soluble Aβ from the brain to the bloodstream, as well as vice versa. Additionally, the ATP-binding cassette transporter P-glycoprotein (P-gp) mediates the translocation of soluble Aβ across neuronal endothelial cells into the circulatory system. Conversely, the gp330/megalin receptor is involved in returning circulating Aβ to the brain through its interaction with apolipoprotein J (ApoJ) [55]. In AD brains, LRP-mediated Aβ efflux is downregulated, while RAGE-mediated influx is upregulated, exacerbating Aβ accumulation. Enzymatic degradation of Aβ is facilitated by various peptidases, notably zinc metalloproteases such as neprilysin and insulin-degrading enzyme (IDE), as well as members of the matrix metalloproteinase (MMP) family, including angiotensin-converting enzyme (ACE) and endothelin-converting enzyme (ECE). Several epidemiological studies have reported that levels and activities of neprilysin, IDE, and ACE are reduced in aging and AD-affected brains [56].

The amyloid precursor protein (APP) is a well-known integral membrane protein localized at neuronal synapses, playing a pivotal role in both Aβ production and its subsequent pathological aggregation. APP spans the lipid bilayer of the neuronal membrane, featuring a large glycosylated extracellular N-terminus and a shorter cytoplasmic C-terminus. Proteolytic processing of human APP occurs via two alternative pathways: amyloidogenic and non-amyloidogenic, both resulting in peptides of varying lengths, including the amyloid β-peptide (Aβ), which consists of 37 to 49 amino acids and is the primary component of amyloid plaques in AD brains [57]. In the amyloidogenic pathway, APP is first cleaved by β-secretase (BACE-1) at the Asp site, producing a membrane-bound C-terminal fragment (C99 or CTFβ) and a secreted N-terminal fragment (sAPPβ). Subsequently, γ-secretase cleaves CTFβ at multiple sites, generating fragments of varying lengths (43, 45, 46, 49, and 51 amino acids), which ultimately lead to the formation of extracellular Aβ peptides, predominantly Aβ40 and Aβ42 [58]. In contrast, the non-amyloidogenic pathway involves cleavage of APP by α-secretase at the Leu site, producing the secreted N-terminal fragment sAPPα and the membrane-bound C-terminal fragment C83 (CTFα). CTFα is further processed by γ-secretase, resulting in the extracellular P3 peptide and CTFγ. These Aβ monomers can aggregate into various forms, including oligomers, protofibrils, and mature amyloid fibrils, which are most commonly observed in the neocortex of AD patients [59].

Post-translational modifications serve as rapid and reversible mechanisms for maintaining protein stability, responding to extracellular stimuli, and facilitating various cellular processes. The SUMO proteins and the sumoylation process were recently discovered and recognized for their significant roles within the cell [6]. SUMO proteins have garnered interest for their roles in both the central and peripheral nervous systems. As a result, research has accelerated on the impact of SUMO proteins and the sumoylation process, a post-translational modification, on neurodegenerative diseases. However, many pathways remain to be elucidated [7].

General Characteristics of SUMO Proteins and Sumoylation:
Discovered in 1996, SUMO, or Small Ubiquitin-Related Modifiers, expresses itself in a variety of eukaryotic cell systems, from yeast and nematodes to fruit flies and mammals [8]. These proteins share an 18% sequence similarity in their three-dimensional structure and function. SUMO proteins, through a metabolic cycle known as sumoylation, play roles in maintaining cellular homeostasis, controlling transcriptional activity, replication, defense responses to factors like inflammation and stress, and regulating gene expression [9]. In yeast and Saccharomyces cerevisiae, there is a single SUMO paralog, Smt3p, while mammals are known to have five paralogs, including SUMO1, SUMO2, SUMO3, and SUMO4. These paralogs have been found to exhibit homology with each other. Molecularly, SUMO2 and SUMO4, and SUMO2 and SUMO3, show homology, whereas functionally, SUMO1 and SUMO4 are homologous. The SUMO proteins' substrates are mostly intracellular proteins. SUMO proteins bind to their substrates via isopeptide bonds, playing roles in numerous biochemical events. Through this binding, they regulate the localization of their substrates within cells, increasing the stability and activity of these proteins [10]. SUMO1, like SUMO2 and SUMO3, shows widespread tissue distribution, but SUMO4 is pre-dominantly found in the spleen, kidney, and lymph nodes [11].

The deconjugation process of SUMO1 is slower than that of SUMO2/3 [12]. Additionally, SUMO-1 is generally found in the nuclear membrane and nucleus, whereas SUMO-2/3 is located in the nucleoplasmic fluid (caryolymph) [11]. SUMO-1 and SUMO-2/3 can act on both the same and different substrates, with studies indicating significant functional differences between them [13]. For example, SUMO-1 forms mono-sumoylation chains, while SUMO-2/3 forms poly-sumoylation chains. SUMO-1 has been shown to serve as a terminal cap in SUMO-2/3 polymer chains [14].

Despite all this information, much remains to be discovered about the recently identified SUMO-4 protein. Studies have shown that SUMO-4 is 86% similar to SUMO-2 [15]. Sumoylation refers to the reversible covalent bonding of any member of the SUMO protein family to lysine groups on substrates (target proteins). To date, over 3,600 SUMO substrates have been identified in sumoylation studies to date [16]. Furthermore, some studies have observed that many proteins bind to SUMOs through non-covalent interactions. This type of binding involves intermediaries known as SUMO interaction motifs (SIMs). These SIM-mediated bonds are especially found in neuronal and synaptic proteins [5]. The bonds formed with target proteins provide temporal and spatial regulation, which is crucial for cell viability. Additionally, studies suggest that disruptions in neuronal sumoylation can lead to or predispose to many diseases [17]. When not in use, SUMO proteins are inactive, and their expression from SUMO genes occurs as inactive precursor molecules [18]

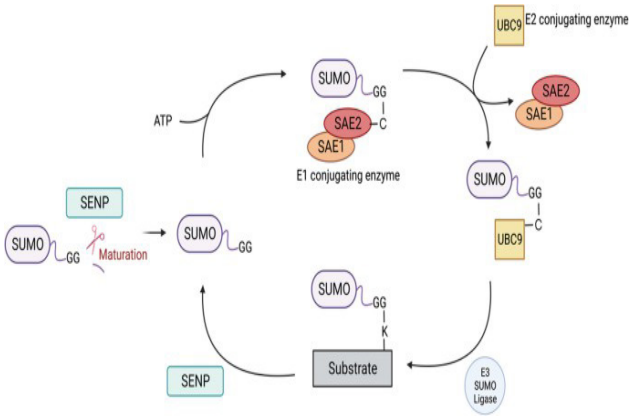

Figure2: Sumoylation Pathway Diagram. (Huang C., Yang T., Lin K.; Journal of Biomedical Science (2024))[52]

As seen in Figure 2, the sumoylation signaling pathway involves the following steps: The function of sumoylation proteins in the sumoylation cycle is assumed to be "protein solubility enhancement." This function has been shown to be effective in regulating protein aggregation and the pathogenesis of neurodegenerative diseases. SUMO has been demonstrated to have direct effects on protein solubility for α-synuclein, DJ-1, Huntington, and STAT1 [19]. The sumoylation process consists of conjugation and deconjugation phases. Three enzymes play key roles in this process: E1 (activating enzyme), E2 (SUMO-specific conjugating enzyme, Ubc9), and E3 (SUMO ligase) [20]. The binding process in mammals begins with the E1 enzyme, a heterodimer of SAE1 and SAE2, activating SUMO proteins in an ATP-dependent manner. During activation, a thioester bond is formed between the glycine residue at the C-terminal of the SUMO protein and the cysteine residue in the active site of SAE2. Immediately after, the SUMO protein is transferred to the active cysteine site of the E2 (Ubc9) conjugating enzyme via the thioester bond [21]. E3 ligase enzymes serve as a bridge between the SUMO-loaded Ubc9 gene and substrate proteins. Additionally, for SUMO transfer to occur, the SUMO-Ubc9 thioester bond must be maintained. SENP enzymes facilitate both sumoylation maturation and deconjugation. Mammals have multiple SENP enzymes. SENP1 and SENP2 enzymes are responsible for the maturation phase of SUMO proteins. Furthermore, these enzymes are involved in breaking the bonds between SUMO-1 and SUMO-2/3 proteins and their substrates. SENP3/5 enzymes are thought to be responsible for monomeric SUMO-2/3 proteins' substrates, while SENP6/7 are involved in the regulation of SUMO-2/3 protein chains [5, 22].

Relationship between SUMO and Ubiquitination

Ubiquitin is a post-translational regulatory protein that consists of approximately 76 amino acids. First identified in 1978, this protein plays a role in various biological pathways. Its primary function is to label proteins for degradation in the 26S proteasomes. Ubiquitination consists of two successive steps: tagging the protein with multiple ubiquitin molecules, and then degrading the tagged protein by the proteasome complex, releasing free or reusable ubiquitin. Generally, ubiquitination and sumoylation share similar enzymatic structures [23].

As previously stated, ubiquitination is a post-translational modification that aims to degrade proteins in the 26S proteasomes by marking them. This process results in the release of free and reusable ubiquitin through two consecutive steps [24] .The ubiquitin systems primarily involve three different enzymes, enabling ubiquitin to covalently bind to substrate proteins or itself from the C-terminus. These enzymes are E1 (activating enzyme), E2 (conjugating enzyme), and E3 (ligating enzyme) [25]. In the first step, E1 activates ubiquitin through an ATP-mediated reaction, resulting in the high-energy thiol ester intermediate E1-S*. The activated ubiquitin is then transferred to a specific substrate via a member of the ubiquitin protein ligase family, E3 ligase, through one of several E2 enzymes, forming the high-energy thiol intermediate E2-S*[26,27] .The E3 enzyme classes, particularly RING-finger-containing types, directly transfer the active ubiquitin from E2 to the substrate bound to E3. In contrast, in HECT domain-containing E3s, the activated ubiquitin is transferred from E2 to the active cysteine residue on E3, forming the high-energy thiol ester intermediate E3-S*, which is subsequently transferred to the ligase-bound substrate. This regulation depends on protein phosphorylation, believed to influence E3 enzyme activity. Ubiquitination typically entails transferring ubiquitin to one of the substrate's seven lysine residues or the N-terminus, forming a covalent isopeptide bond that results in a variety of ubiquitin chain types and lengths [28]. Numerous ubiquitination types exist, forming different structured chains based on binding types recognized as specific signals by ubiquitin-binding proteins, which regulate the modified protein's enzymatic activity, stability, and localization [29] .

The molecular diagrams of ubiquitin, SUMO1, SUMO2, and SMT3, the single SUMO paralog found in Saccharomyces cerevisiae, are provided in Figure 3. (referee1 reccomendation.)

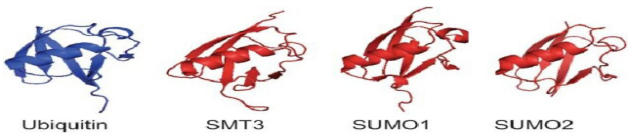

Figure 3: A Diagram of SUMO paralogue and Ubiquitin. (Alonso A., Greenlee M. Et al.; Cytoskeleton, 2015.)[49]

SUMO Protein Family and Alzheimer's Disease

Risk factors for AD include age, gender, dementia, genetic factors (presence of the Apolipoprotein E (Apo E) e4 gene), Down syndrome, atherosclerosis, diabetes mellitus, systemic diseases, metabolic factors (amyloid-β metabolism), hypertension and hypotension, smoking, infectious factors, poisoning, history of major depression, and head trauma [31, 32]. As they age, people may experience forgetfulness, slower speech, fatigue, and unhappiness, which can be normal aging signs or symptoms of AD. AD significantly complicates patient lives, leading to substantial declines in quality of life [33].

The clinical course of AD is divided into three stages based on the severity of symptoms and findings: Early stage, middle stage, and advanced stage. The early stage is characterized by memory disorders, difficulty learning new information, repeatedly asking questions, and misplacing items [34]. Since

forgetfulness is considered normal in elderly individuals, there can be delays in seeking medical help, resulting in a late diagnosis. In the middle stage, there is a functional loss in many daily activities due to the worsening of early-stage symptoms [35]. Information from the recent past starts to fade slowly. Patients may get lost when going out and become unable to manage financial processes. In the advanced stage, patients require assistance with basic daily activities. "2023 Alzheimer's Disease Facts and Figures" mentions that patients become completely dependent on basic needs such as dressing, bathing, and eating. Communication is reduced to meaningless sounds and words, making understanding the patient difficult. Complications from diseases like pulmonary embolism, bed sore infections, and nutritional disorders are among the primary causes of death [36].

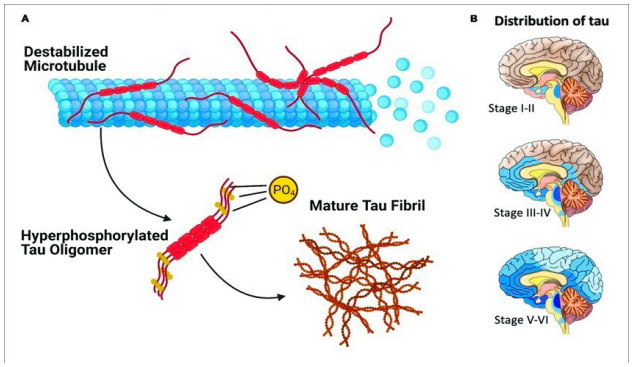

Figure 4: A Diagram of Alzheimer's Disease and Tau Proteins Aggregation Motifs, (Mah D., Zhao J. Et al.; Frontiers in Molecular Biosciences, 2021.)[50]

As shown in Figure 4, alzheimer's disease is a progressive condition characterized by neuron and synapse loss in certain parts of the central nervous system (CNS). Genetic predisposition is a significant factor in AD development. It is a complex disease that presents at multiple levels and is influenced by various pathways. Two primary pathological findings in AD are amyloid plaques and neurofibrillary tangles [37]. Genes associated with AD include amyloid precursor protein (APP), Presenilin 1 (PS1), Presenilin 2 (PS2) (responsible for AD before age 65), and ApoE (responsible for AD after age 65) [38]. The APP gene is located on chromosome 21, and the PS2 genes are on chromosome 1. Mutations in these chromosomal regions increase amyloid-β peptide levels in AD. These mutations result in abnormal APP cleavage, toxic amyloid-β production, Tau protein hyperphosphorylation, and neurofibrillary tangle (NFT) formation. Early-onset AD develops due to APP (2–3%), PS1 (70–80%), and PS2 (20%) gene mutations [35].

For late-onset AD, the ApoE gene on chromosome 19 is influential. The e2 allele of this gene is protective and reduces AD risk, while the ApoE e4 allele increases AD risk by promoting amyloid plaque and NFT formation. Mutations in the ApoE gene account for 50–80% of late-onset AD. However, ApoE e4 alone is not sufficient to cause AD [36]. The most known pathological finding in AD is amyloid plaques. Amyloid-β peptides, which result from the proteolytic breakdown of the amyloid precursor protein, are linked to the disease. The APP protein is metabolized by proteolytic enzymes called α-, β-, and γ-secretases. In the first step, APP is cleaved by either α-secretase (non-toxic, normal cleavage) or β-secretase (toxic, abnormal cleavage). Subsequently, γ-secretase generates amyloid-β and AICD (APP intracellular domain) fragments from C99 [39].

Current methods do not offer an effective therapeutic pathway to alter disease progression or slow or halt cognitive decline. To address this gap, a better understanding of the disrupted signaling pathways underlying AD pathology, including the regulatory mechanisms that typically control these networks, is essential. One such mechanism involves sumoylation, a post-translational modification that regulates many aspects of cell biology and has several critical neuron-specific roles. Connections with the ubiquitin proteasome system (UPS) and, more recently, autophagy have been a focal point [40]. Conjugation with SUMO and the pathways regulated by SUMO have been less studied in relation to AD pathology and neuronal physiology. However, sumoylation's involvement in these areas has gained momentum in recent years [41]. The diagram in Figure 5, illustrating the roles of Alzheimer's disease and SUMO proteins, also supports this paragraph. (Referee1 Reccomendations.)

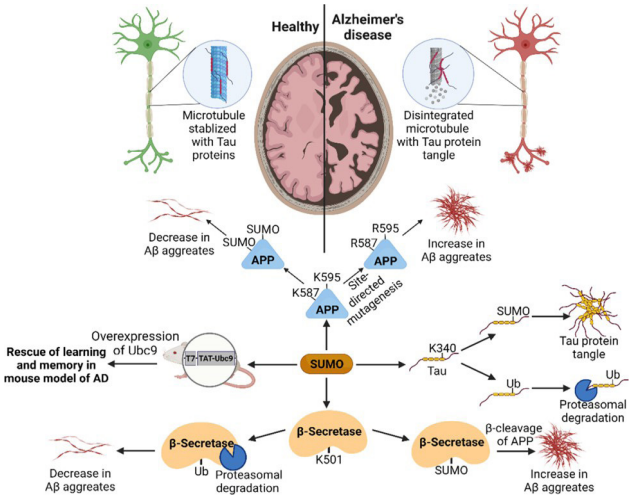

Figure 5: A Diagram of Alzheimer Disease's and SUMO Proteins. (Mandel N., Agarwal N.; Cells, 2022.)[51]

Given the numerous proteins subjected to sumoylation in neurons, it is unsurprising that any disruption in this post-translational modification affects Alzheimer's disease [42, 43, 44]. Evidence from genetic studies supports this hypothesis. A single nucleotide polymorphism (SNP) on chromosome 6 (rs6907175) linked to the SUMO-activating enzyme (E1) subunit 2 homolog (SAE2) has been found to be significantly associated with AD in multiple independent sample sets. The SNP was later confirmed to be significant in another genetic study on sporadic AD [45].The mechanism by which the SAE2 homolog SNP influences AD pathogenesis is unclear.

Another SUMO enzyme, protease SENP3, showed altered expression in microarray analyses of the inferior parietal lobules of sporadic AD patients [46]. In AD, there is a significant downregulation of SENP3 expression; RT-PCR confirmed that

AD tissue had about half the average SENP3 expression of controls. The SUMO-conjugated enzyme Ubc9 is the third sumoylation protein linked to AD. Genomic DNA analysis of late-onset AD patients revealed an SNP (rs761059) in intron 7 of the Ubc9 gene (UBE2I) that is significantly associated with the disease [47,48]. These studies indicate that changes in sumoylation likely play a role in AD, although research into the underlying mechanisms continues.

Conclusion and Recommendations

This review has examined the precise impacts of the SUMO protein family on Alzheimer's disease, with a focus on the noteworthy influence of post-translational modification systems on intricate neurodegenerative conditions. The SUMO system is a post-translational modification system that has significant involvement in the development of neurodegenerative illnesses. This involvement occurs via its metabolic cycles, which are referred to as sumoylation. Although the significance of these systems has been recently uncovered, they have been discovered to play a crucial role in the development of several disorders. SUMOs, via a metabolic cycle and processes akin to ubiquitination, govern cellular function by managing factors such as intracellular localization and protein homeostasis resulting from gene expression. A thorough investigation and future discoveries about these routes are essential. Gaining a comprehensive understanding of SUMO pathways would greatly enhance the progress of research aimed at developing therapies for complex neurodegenerative illnesses such as Alzheimer's, which now lack a definite cure.

References

1. Wilson, D. M., Cookson, M. R., van den Bosch, L., Zetterberg, H., Holtzman, D. M., & Dewachter, I. (2023). Hallmarks of neurodegenerative diseases. In Cell (Vol. 186, Issue 4). https://doi.org/10.1016/j.cell.2022.12.032
2. Yau, T. Y., Molina, O., & Courey, A. J. (2020). SUMOylation in development and neurodegeneration. Development(Cambridge), 147(6). https://doi.org/10.1242/dev.175703
3. Dorval, V., & Fraser, P. E. (2007). SUMO on the road to neurodegeneration. In Biochimica et Biophysica Acta - Molecular Cell Research (Vol. 1773, Issue 6). https://doi.org/10.1016/j.bbamcr.2007.03.017
4. Slanzi, A., Iannoto, G., Rossi, B., Zenaro, E., & Constantin, G. (2020). In vitro Models of Neurodegenerative Diseases. In Frontiers in Cell and Developmental Biology (Vol. 8). https://doi.org/10.3389/fcell.2020.00328
5. Song, J., Durrin, L. K., Wilkinson, T. A., Krontiris, T. G., & Chen, Y. (2004). Identification of a SUMO-binding motif that recognizes SUMO-modified proteins. Proceedings of the National Academy of Sciences of the United States of America, 101(40). https://doi.org/10.1073/pnas.0403498101
6. Correa-Vázquez, J. F., Juárez-Vicente, F., García-Gutiérrez, P., Barysch, S. v., Melchior, F., & García-Domínguez, M. (2021). The Sumo proteome of proliferating and neuronal- differentiating cells reveals Utf1 among key Sumo targets involved in neurogenesis. Cell Death and Disease, 12(4). https://doi.org/10.1038/s41419-021-03590-2
7. Mandel, N., & Agarwal, N. (2022). Role of SUMOylation in Neurodegenerative Diseases. In Cells (Vol. 11, Issue 21). https://doi.org/10.3390/cells11213395
8. Küçükali, C. I., Salman, B., Yüceer, H., Ulusoy, C., Abacı, N., Ekmekci, S. S., Tüzün, E., Bilgiç, B., & Hanağası, H. A. (2020). Small ubiquitin-related modifier (SUMO) 3 and SUMO4 gene polymorphisms in Parkinson's disease. Neurological Research, 42(6). https://doi.org/10.1080/01616412.2020.1724464
9. Soares, E. S., Prediger, R. D., Brocardo, P. S., & Cimarosti, H. I. (2022). SUMO- modifying Huntington's disease. In IBRO Neuroscience Reports (Vol. 12). https://doi.org/10.1016/j.ibneur.2022.03.002
10. Şen, M., Ay, U., Akbayır, E., Şenyer, S., Tüzün, E., & Küçükali, C. İ. (2017). NF-kB, SUMO ve Ubikitinasyon İlişkisi NF-κB SUMO AND UBIQUITINATION RELATIONSHIP. Deneysel Tıp Araştırma Enstitüsü Dergisi, 7(13).
11. Yuan, H., Zhou, J., Deng, M., Liu, X., le Bras, M., de The, H., Chen, S. J., Chen, Z., Liu, T. X., & Zhu, J. (2010). Small ubiquitin-related modifier paralogs are indispensable but functionally redundant during early development of zebrafish. Cell Research, 20(2). https://doi.org/10.1038/cr.2009.101
12. Kolli, N., Mikolajczyk, J., Drag, M., Mukhopadhyay, D., Moffatt, N., Dasso, M., Salvesen, G., & Wilkinson, K. D. (2010). Distribution and paralogue specificity of mammalian deSUMOylating enzymes. Biochemical Journal, 430(2). https://doi.org/10.1042/BJ20100504
13. Yang, W. S., Hsu, H. W., Campbell, M., Cheng, C. Y., & Chang, P. C. (2015). K-bZIP Mediated SUMO-2/3 Specific Modification on the KSHV Genome Negatively Regulates Lytic Gene Expression and Viral Reactivation. PLoS Pathogens, 11(7). https://doi.org/10.1371/journal.ppat.1005051
14. Matic, I., van Hagen, M., Schimmel, J., Macek, B., Ogg, S. C., Tatham, M. H., Hay, R. T., Lamond, A. I., Mann, M., & Vertegaal, A. C. O. (2008). In vivo identification of human small ubiquitin-like modifier polymerization sites by high accuracy mass spectrometry and an in vitro to in vivo strategy. Molecular and Cellular Proteomics, 7(1). https://doi.org/10.1074/mcp.M700173-MCP200
15. Owerbach, D., McKay, E. M., Yeh, E. T. H., Gabbay, K. H., & Bohren, K. M. (2005). A proline-90 residue unique to SUMO-4 prevents maturation and sumoylation. Biochemical and Biophysical Research Communications, 337(2). https://doi.org/10.1016/j.bbrc.2005.09.090
16. Wang, W.; Matunis, M.J. Paralogue-Specific Roles of SUMO1 and SUMO2/3 in Protein Quality Control and Associated Diseases. Cells 2024, 13, 8. https://doi.org/10.3390/cells13010008
17. Hayashi, T., Seki, M., Maeda, D., Wang, W., Kawabe, Y. I., Seki, T., Saitoh, H., Fukagawa, T., Yagi, H., & Enomoto, T. (2002). Ubc9 is essential for viability of higher eukaryotic cells. Experimental Cell Research, 280(2). https://doi.org/10.1006/excr.2002.5634
18. Lamoliatte, F., Bonneil, E., Durette, C., Caron-Lizotte, O., Wildemann, D., Zerweck, J., Wenshuk, H., & Thibault, P. (2013). Targeted identification of SUMOylation sites in human proteins using affinity enrichment and paralog-specific reporter ions. Molecular and Cellular Proteomics, 12(9). https://doi.org/10.1074/mcp.M112.025569
19. Krumova, P., Meulmeester, E., Garrido, M., Tirard, M., Hsiao, H. H., Bossis, G., Urlaub, H., Zweckstetter, M., Kügler, S., Melchior, F., Bähr, M., & Weishaupt, J. H. (2011). Sumoylation inhibits α-synuclein aggregation and toxicity. Journal of Cell Biology, 194(1). https://doi.org/10.1083/jcb.201010117
20. Chang, C. C., Naik, M. T., Huang, Y. S., Jeng, J. C., Liao, P. H., Kuo, H. Y., Ho, C. C., Hsieh, Y. L., Lin, C. H., Huang, N. J., Naik, N. M., Kung, C. C. H., Lin, S. Y., Chen, R. H., Chang, K. S., Huang, T. H., & Shih, H. M. (2011). Structural and Functional Roles of Daxx SIM Phosphorylation in SUMO Paralog-Selective Binding and Apoptosis Modulation. Molecular Cell, 42(1). https://doi.org/10.1016/j.molcel.2011.02.022
21. Wilkinson, K. A., & Henley, J. M. (2010). Mechanisms, regulation and consequences of protein SUMOylation. In Biochemical Journal (Vol. 428, Issue 2). https://doi.org/10.1042/BJ20100158
22. Zhang, F.-P., Mikkonen, L., Toppari, J., Palvimo, J. J., Thesleff, I., & Jänne, O. A. (2008). Sumo-1 Function Is Dispensable in Normal Mouse Development . Molecular and Cellular Biology, 28(17). https://doi.org/10.1128/mcb.00651-08

23. Husnjak, K., & Dikic, I. (2012). Ubiquitin-binding proteins: Decoders of ubiquitin- mediated cellular functions. Annual Review of Biochemistry, 81. https://doi.org/10.1146/annurev-biochem-051810-094654
24. Kamitani, T., Kito, K., Nguyen, H. P., Fukuda-Kamitani, T., & Yeh, E. T. H. (1998). Characterization of a second member of the sentrin family of ubiquitin- like proteins. Journal of Biological Chemistry, 273(18). https://doi.org/10.1074/jbc.273.18.11349
25. Varshavsky, A. (2006). The early history of the ubiquitin field. Protein Science, 15(3). https://doi.org/10.1110/ps.052012306
26. Gill, G. (2004). SUMO and ubiquitin in the nucleus: Different functions, similar mechanisms? In Genes and Development(Vol. 18, Issue 17). https://doi.org/10.1101/gad.1214604
27. Hendriks, I. A., Akimov, V., Blagoev, B., & Nielsen, M. L. (2021). MaxQuant.Live Enables Enhanced Selectivity and Identification of Peptides Modified by Endogenous SUMO and Ubiquitin. Journal of Proteome Research, 20(4). https://doi.org/10.1021/acs.jproteome.0c00892
28. Sriramachandran, A. M., & Dohmen, R. J. (2014). SUMO-targeted ubiquitin ligases. In Biochimica et Biophysica Acta - Molecular Cell Research (Vol. 1843, Issue 1). https://doi.org/10.1016/j.bbamcr.2013.08.022
29. Keiten-Schmitz, J., Wagner, K., Piller, T., Kaulich, M., Alberti, S., & Müller, S. (2020). The Nuclear SUMO-Targeted Ubiquitin Quality Control Network Regulates the Dynamics of Cytoplasmic Stress Granules. Molecular Cell, 79(1). https://doi.org/10.1016/j.molcel.2020.05.017
30. Adalı, A. , Y. A. , K. B. , E. P. (2020). (2020). ALZHEİMER HASTALIĞININ GELİŞİMİNDE BİYOLOJİK AJANLARIN OLASI ETKİLERİ. Journal of Faculty of Pharmacy of Ankara University, 44(1), 167-187. , 167–187.
31. Wang, J., Gu, B. J., Masters, C. L., & Wang, Y. J. (2017). A systemic view of Alzheimer disease - Insights from amyloid-β metabolism beyond the brain. In Nature Reviews Neurology (Vol. 13, Issue 10). https://doi.org/10.1038/nrneurol.2017.111
32. Özpak, L., Pazarbaşı, A., & Keser, N. (2017). Alzheimer Hastalığının Genetiği ve Epigenetiği. Arşiv Kaynak Tarama Dergisi, 26(1). https://doi.org/10.17827/aktd.280520
33. Trejo-Lopez, J. A., Yachnis, A. T., & Prokop, S. (2022). Neuropathology of Alzheimer's Disease. In Neurotherapeutics(Vol. 19, Issue 1). https://doi.org/10.1007/s13311-021- 01146-y
34. Tahami Monfared, A. A., Byrnes, M. J., White, L. A., & Zhang, Q. (2022). Alzheimer's Disease: Epidemiology and Clinical Progression. In Neurology and Therapy (Vol. 11, Issue 2). https://doi.org/10.1007/s40120-022-00338-8
35. Porsteinsson, A. P., Isaacson, R. S., Knox, S., Sabbagh, M. N., & Rubino, I. (2021). Diagnosis of Early Alzheimer's Disease: Clinical Practice in 2021. In Journal of Prevention of Alzheimer's Disease (Vol. 8, Issue 3). https://doi.org/10.14283/jpad.2021.23
36. Zhang, X. X., Tian, Y., Wang, Z. T., Ma, Y. H., Tan, L., & Yu, J. T. (2021). The Epidemiology of Alzheimer's Disease Modifiable Risk Factors and Prevention. In Journal of Prevention of Alzheimer's Disease (Vol. 8, Issue 3). https://doi.org/10.14283/jpad.2021.15
37. Deture, M. A., & Dickson, D. W. (2019). The neuropathological diagnosis of Alzheimer's disease. In Molecular Neurodegeneration (Vol. 14, Issue 1). https://doi.org/10.1186/s13024-019-0333-5
38. Weller, J., & Budson, A. (2018). Current understanding of Alzheimer's disease diagnosis and treatment.I n F1000Research (Vol. 7). https://doi.org/10.12688/f1000research.14506.1
39. Chen, Z. R., Huang, J. B., Yang, S. L., & Hong, F. F. (2022). Role of Cholinergic Signaling in Alzheimer's Disease. In Molecules (Vol. 27, Issue 6). https://doi.org/10.3390/molecules27061816
40. Jeong, D. U., Lee, J. E., Lee, S. E., Chang, W. S., Kim, S. J., & Chang, J. W. (2014). Improvements in memory after medial septum stimulation are associated with changes in hippocampal cholinergic activity and neurogenesis. BioMed Research International, 2014. https://doi.org/10.1155/2014/568587
41. Lee, L., Sakurai, M., Matsuzaki, S., Arancio, O., & Fraser, P. (2013). SUMO and alzheimer's disease. In NeuroMolecular Medicine (Vol. 15, Issue 4). https://doi.org/10.1007/s12017-013-8257-7
42. Liang, Z., Chan, H. Y. E., Lee, M. M., & Chan, M. K. (2021). A SUMO1-Derived Peptide Targeting SUMO-Interacting Motif Inhibits α-Synuclein Aggregation. Cell Chemical Biology, 28(2). https://doi.org/10.1016/j.chembiol.2020.12.010
43. Hong, Y., Rogers, R., Matunis, M. J., Mayhew, C. N., Goodson, M., Park-Sarge, O. K., & Sarge, K. D. (2001). Regulation of Heat Shock Transcription Factor 1 by Stress- induced SUMO-1 Modification. Journal of Biological Chemistry, 276(43). https://doi.org/10.1074/jbc.M104714200
44. Sarge, K. D., & Park-Sarge, O. K. (2005). Gene bookmarking: Keeping the pages open. In Trends in Biochemical Sciences (Vol. 30, Issue 11). https://doi.org/10.1016/j.tibs.2005.09.004
45. Sarge, K. D., & Park-Sarge, O. K. (2009). Sumoylation and human disease pathogenesis. In Trends in Biochemical Sciences (Vol. 34, Issue 4). https://doi.org/10.1016/j.tibs.2009.01.004
46. Holton, P., Ryten, M., Nalls, M., Trabzuni, D., Weale, M. E., Hernandez, D., Crehan, H., Gibbs, J. R., Mayeux, R., Haines, J. L., Farrer, L. A., Pericak-Vance, M. A., Schellenberg, G. D., Ramirez-Restrepo, M., Engel, A., Myers, A. J., Corneveaux, J. J., Huentelman, M. J., Dillman, A., … Guerreiro, R. (2013). Initial Assessment of the Pathogenic Mechanisms of the Recently Identified Alzheimer Risk Loci. Annals of Human Genetics, 77(2). https://doi.org/10.1111/ahg.12000
47. Vijayakumaran, S., Wong, M. B., Antony, H., & Pountney, D. L. (2015). Direct and/or indirect roles for SUMO in modulating alpha-synuclein toxicity. In Biomolecules (Vol. 5, Issue 3). https://doi.org/10.3390/biom5031697
48. Ahner, A., Gong, X., & Frizzell, R. A. (2016). Divergent signaling via SUMO modification: Potential for CFTR modulation. In American Journal of Physiology - Cell Physiology (Vol. 310, Issue 3). https://doi.org/10.1152/ajpcell.00124.2015
49. Alonso, A., Greenlee, M., Matts, J., Kline, J., Davis, K. J., & Miller, R. K. (2015). Emerging roles of sumoylation in the regulation of actin, microtubules, intermediate filaments, and septins. In Cytoskeleton (Vol. 72, Issue 7). https://doi.org/10.1002/cm.21226
50. Mah, D., Zhao, J., Liu, X., Zhang, F., Liu, J., Wang, L., Linhardt, R., & Wang, C. (2021). The Sulfation Code of Tauopathies: Heparan Sulfate Proteoglycans in the Prion Like Spread of Tau Pathology. In Frontiers in Molecular Biosciences (Vol. 8). https://doi.org/10.3389/fmolb.2021.671458
51. Mandel, N., & Agarwal, N. (2022). Role of SUMOylation in Neurodegenerative Diseases. In Cells (Vol. 11, Issue 21). https://doi.org/10.3390/cells11213395
52. Huang, C. H., Yang, T. T., & Lin, K. I. (2024). Mechanisms and functions of SUMOylation in health and disease: a review focusing on immune cells. In Journal of Biomedical Science (Vol. 31, Issue 1). https://doi.org/10.1186/s12929-024-01003-y
53. Reiman, E. M., Arboleda-Velasquez, J. F., Quiroz, Y. T., Huentelman, M. J., Beach, T. G., Caselli, R. J., Chen, Y., Su, Y., Myers, A. J., Hardy, J., Paul Vonsattel, J., Younkin, S. G., Bennett, D. A., De Jager, P. L., Larson, E. B., Crane, P. K., Keene, C. D., Kamboh, M. I., Kofler, J. K., Duque, L., … Alzheimer's Disease Genetics Consortium (2020). Exceptionally low likelihood of Alzheimer's dementia in APOE2 homozygotes from a 5,000-person neuropathological study. Nature communications, 11(1), 667. https://doi.org/10.1038/s41467-019-14279-8
54. Baranello, R. J., Bharani, K. L., Padmaraju, V., Chopra, N., Lahiri, D. K., Greig, N. H., Pappolla, M. A., & Sambamurti, K. (2015). Amyloid-beta protein clearance and degradation (ABCD) pathways and their role in Alzheimer's disease. Current Alzheimer research, 12(1), 32–46. https://doi.org/10.2174/1567205012666141218140953
55. Chen, G. F., Xu, T. H., Yan, Y., Zhou, Y. R., Jiang, Y., Melcher, K., & Xu, H. E. (2017). Amyloid beta: structure, biology and structure-based therapeutic development. Acta pharmacologica Sinica, 38(9), 1205–1235. https://doi.org/10.1038/aps.2017.28

56. Malpetti, M., Kievit, R. A., Passamonti, L., Jones, P. S., Tsvetanov, K. A., Rittman, T., Mak, E., Nicastro, N., Bevan-Jones, W. R., Su, L., Hong, Y. T., Fryer, T. D., Aigbirhio, F. I., O'Brien, J. T., & Rowe, J. B. (2020). Microglial activation and tau burden predict cognitive decline in Alzheimer's disease. Brain : a journal of neurology, 143(5), 1588–1602. https://doi.org/10.1093/brain/awaa088
57. Hayden, E. Y., & Teplow, D. B. (2013). Amyloid β-protein oligomers and Alzheimer's disease. Alzheimer's research & therapy, 5(6), 60. https://doi.org/10.1186/alzrt226
58. Fagiani, F., Lanni, C., Racchi, M., & Govoni, S. (2021). (Dys) regulation of Synaptic Activity and Neurotransmitter Release by β-Amyloid: A Look Beyond Alzheimer's Disease Pathogenesis. Frontiers in molecular neuroscience, 14, 635880. https://doi.org/10.3389/fnmol.2021.635880
59. Ali, J.; Choe, K.; Park, J.S.; Park, H.Y.; Kang, H.; Park, T.J.; Kim, M.O. The Interplay of Protein Aggregation, Genetics, and Oxidative Stress in Alzheimer's Disease: Role for Natural Antioxidants and Immunotherapeutics. Antioxidants 2024, 13, 862. https://doi.org/10.3390/antiox13070862
60. Vignon, A., Salvador-Prince, L., Lehmann, S., Perrier, V., & Torrent, J. (2021). Deconstructing alzheimer's disease: How to bridge the gap between experimental models and the human pathology? In International Journal of Molecular Sciences(Vol. 22, Issue 16). https://doi.org/10.3390

HİTİT JOURNAL OF SCIENCE

e-ISSN: 3061-9629
Volume: 2 • Number: 1
January 2025

Voltammetric Determination of Lead on The Bismuth Coated Glassy Carbon Electrode Surface in Sugar Beet Washing Water

Burcu Yılmaz | Ebru Gökmeşe* | Faruk Gökmeşe

Department of Chemistry, Hitit University, 19030,Çorum, Türkiye.

Corresponding Author

Ebru Gökmeşe
E-mail: ebrugokmese@hitit.edu.tr Phone: +90 364 227 7000
RORID: ror.org/01x8m3269

Article Information

Article Type: Research Article
Doi: -
Received: 16.07.2024
Accepted: 20.11.2024
Published: 31.01.2025

Cite As

Yılmaz B., et al. Voltammetric Determination of Lead on The Bismuth Coated Glassy Carbon Electrode Surface in Sugar Beet Washing Water. 2025;2(1):9-17.

Peer Review: Evaluated by independent reviewers working in at least two different institutions appointed by the field editor.
Ethical Statement: Not available.
Plagiarism Checks: Yes - iThenticate
Conflict of Interest: Authors approve that to the best of their knowledge, there is not any conflict of interest or common interest with an institution/ organization or a person that may affect the review process of the paper.

CRedit Author Statement
Beyza AYDIN: Design of the study, writing, reviewing, editing, supervisio

Voltammetric Determination of Lead on The Bismuth Coated Glassy Carbon Electrode Surface in Sugar Beet Washing Water

Burcu Yılmaz | Ebru Gökmeşe* | Faruk Gökmeşe
Department of Chemistry, Hitit University, 19030,Çorum, Türkiye

Abstract
In this project, a new voltammetric method for the lead (Pb) heavy metal in the washing water obtained from the sugar beet washing step that is one of the stages of the process using in sugar plants have been developed. The working electrode was produced by coating a commercial glassy carbon electrode with bismuth. A new analytical method has been enhanced for quantitative analysis of lead in 0.1 M KNO_3 in acetate buffer by using square wave anodic stripping voltammetry (SWASV). It was found that the new bizmuth electrode could work with 0.01 µM as the limit of quantitation and in 0.1 µM – 1 µM concentration range as linear working range.

Keywords: Lead, Square Wave Voltammetry, Heavy Metal, Bismuth Electrode.

INTRODUCTION
Voltammetry, one of the electroanalytical techniques, is a potential-controlled technique where the net current is different from zero. In the mid-1960s, several advantages were sought when selecting voltammetric methods for determinations. With its low cost, high sensitivity, and ease of application, interest in these methods has increased for the determination of many species, particularly in pharmaceutical, environmental, and biological contexts (Yavaş, 2014).

The validation of bismuth film electrodes for the determination of cobalt and cadmium in soil samples has been studied. Bismuth film electrodes were used either by in-situ coating or by being pre-prepared. The deposition potential was set at -1.0 V and the deposition time at 120 s with 0.1 M acetate buffer. While determining cobalt, the bismuth film electrode was prepared in a separate solution. A glassy carbon electrode was immersed in a solution containing 0.1 M acetate buffer and 100 mg/L Bi(III) and stirred for 5 minutes at -1.0 V (Hutton, 2004).

Economou (2005) has compiled a review on the recent developments of bismuth film electrodes. He noted that the conditions for bismuth film coating could vary, suggesting an acidic medium since bismuth may hydrolyze at high pH. He mentioned that coating could be performed by stirring a solution containing 5-200 mg/L Bi(III) at -0.5 to -1.2 V for 1-8 minutes. For instant coating, he emphasized that Bi(III) ions in the range of 400-1000 mg/L could be directly added to the sample. Another method is the bulk modification of the electrode with Bi_2O_3 at -1.0 V. Bi_2O_3 is reduced to metallic bismuth and can accumulate on the electrode surface (Economou, 2005).

Gentamicin selective electrode, poly β-cyclodextrin-p-toluene sulfonic acid/glassy carbon electrode was prepared by electropolymerization technique. Characterization of the prepared poly p-cyclodextrin-p-toluene sulfonic acid/glassy carbon electrode was carried out using cyclic voltammetry and electrochemical impedance spectroscopy. Then, the effects of various parameters were investigated using square wave anodic stripping voltammetry in citrate buffer containing 4.0 $mmolL^{-1}$ gentamicin. From the calibration chart, the correlation coefficient and detection limit were obtained as 0.9999 and 3.7 $\mu molL^{-1}$, respectively (Burç, 2024).
A novel Pb^{2+} selective sensor based on ionic imprinted polymer has been investigated using differential pulse voltammetry (DPV) for the determination of trace lead levels in natural water and fruit juice. The new polymer was used to modify a GCE to create a new electrochemical sensor. Highly suitable voltammetric performance was achieved for the electrochemical detection of lead with a low detection limit (0.05 $ngmL^{-1}$) over a wide linear concentration range (0.1–80 $ngmL^{-1}$) (Dahaghin, 2020).

In another study, where bismuth electrodes were prepared by the direct addition of 400 ppb (µg/L) bismuth (III) to the sample, bismuth and the target metal were deposited on glassy carbon or carbon fiber material. Using stripping voltammetry, Cd, Pb, and Zn were determined at microgram per liter levels (Wang, 2000).

The bismuth electrode was investigated as an alternative electrode for the analysis of Pb, Cd, and Zn in anodic stripping voltammetry. In this study, the electrode was prepared by coating it with bismuth, yielding results with similar sensitivity to those obtained with bismuth-based electrodes. Metal accumulation was conducted using a square wave voltammetric stripping technique from -1.4 V to 0.35 V for 180 seconds. Detection limits of 93, 54, and 396 ng/L were obtained for Pb(II), Cd(II), and Zn(II), respectively, within a calibration range of 10-100 µg/L. The optimized method successfully determined heavy metals in river water using bismuth as an alternative electrode (Kristie, 2010).

Lead is the first metal to cause significant damage to the ecological system through human activities. It is a soft metal with a bluish or silver-gray color. Lead is the most important heavy metal causing environmental pollution, as it is released into the atmosphere in the form of metal or compounds, both of which exhibit toxic properties. According to the World Health Organization (WHO), the permissible limit in the workplace is 0.1 mg/m^3 (Özkan, 2009).

According to Özbolat (2016), lead is a heavy metal and neurotoxin that does not participate in biochemical reactions and has been known and used by humans for thousands of years. It is one of the most significant heavy metals threatening human health. Inorganic lead is found in the atmosphere as particles, whereas organic lead is volatile and often contaminates food and drinking water. Therefore, organic lead affects living organisms more than inorganic lead. The widespread industrial use and prevalence in environmental elements make lead a significant exposure factor both

environmentally and occupationally (Gülçin, 2002).

Lead exposure occurs through environmental and industrial pathways (Özbolat and Tuli, 2016). A significant portion of environmental lead pollution originates from tetraethyl lead, which is released from the combustion of gasoline used in motor vehicles. Lead contamination in marine life is observed as a result of industrial waste being transported by water. For lead to have a toxic effect in the body, it must accumulate to a certain level in the blood or soft tissues. The impact varies depending on several factors, such as age, nutrition, and physiological conditions. For children, toxic symptoms can be observed at 40-80 µg Pb/100 mL, and lead poisoning occurs at 80 µg Pb/100 mL.

The concentration of lead detected in waters close to metal industries is higher compared to other waters. The chemical form of lead plays a significant role in its biological effects. For example, lead tetraethyl can easily diffuse through the skin and mucous membranes into the body. Only 5-10% of lead entering the digestive system enters the bloodstream. About 30-40% of lead taken in through the respiratory tract enters the bloodstream. Once in the bloodstream, some lead accumulates in bones, while the rest is excreted in urine. This mechanism prevents lead accumulation in soft tissues. Lead inhibits the synthesis of hemoglobin, a crucial component of red blood cells, leading to anemia. Reduced red blood cell synthesis results in anemia in poisoned individuals. Studies on adults generally show low levels of lead in the blood (Gündüz, 1998).

In humans, acute lead poisoning can lead to brain damage and death, while chronic poisoning, to which infants and children are particularly sensitive, can result in intellectual impairment, learning disabilities, hyperactivity, hypertension, chronic anemia, and peripheral nerve damage from early exposure to lead (Çağlarırmak and Hepçimen, 2010). These heavy metals also enter the bodies of all living organisms through the food chain and can cause serious damage to organs when consumed in excessive amounts. Therefore, in today's industrial production, the importance of treating industrial wastewater in compliance with standards has become even more crucial (Dinç and Yılmaz, 2013).

This study aims to develop a practical, cost-effective, and rapid analysis method for determining the amount of lead in untreated sugar beet washing water entering a wastewater treatment plant. For this purpose, voltammetric stripping technique, known for its cost advantages in terms of equipment and consumables, as well as its repeatability, will be employed. There are numerous studies in the literature on the voltammetric determination of heavy metals in various samples. However, mercury electrodes have been predominantly used in existing studies. Mercury electrodes are considered the most successful electrodes due to their large surface area, high sensitivity, good repeatability, and renewability. However, awareness of environmental protection has led to a reduction in mercury electrode applications. Due to the toxic effects of mercury, recent studies have focused on alternative electrode materials. Particularly, bismuth-based electrodes are suggested for use in the voltammetric stripping technique for the determination of heavy metals.

Bismuth film electrodes have become attractive to electroanalytical researchers in the past decade. These electrodes are important for maintaining the negligible toxicity of bismuth and its salts, while preserving all the advantages of mercury film electrodes (Huang, 2012). In the proposed study, experiments were conducted to produce a new bismuth electrode based on literature findings. The usability of the obtained electrode for heavy metal determination was investigated. By employing new methods during the metal accumulation and stripping stages, the aim was to develop a new method with lower detection limits and a wider working range compared to previous studies.

Since lead is a heavy metal that is harmful to human health, waste should be controlled and the amount of lead released into the environment should be monitored. By preventing contamination of soil and water resources, toxic substances can be prevented from entering the food chain in agricultural activities.

Because environmental protection laws and regulations require industrial wastes to be managed in accordance with certain standards, lead determination is necessary to comply with these regulations.

Lead from sources such as industrial waste and vehicle exhaust can migrate into the soil and disrupt the ecosystem. In addition, it may leak into water sources, threatening drinking water quality and causing dangerous consequences for human health. Lead exposure, especially in children, can negatively affect brain development, leading to learning disabilities, attention deficits, and behavioral problems. In adults, lead may increase the risk of high blood pressure and other cardiovascular diseases. Long-term lead exposure can cause deterioration in kidney function. Lead can inhibit the production of blood cells, leading to anemia.

MATERIAL AND METHODS

Reagents

All chemicals used in the experimental stage [$Pb(NO_3)_2$, $BiCl_3$, CH_3COOH, KNO_3, NaOH, ferrosen, dopamine, KCl, ACN, NaCl, H_2SO_4] were procured from Sigma-Aldrich. 0.05 M $BiCl_3$ (Reidel de Haen) solution and 0.2 M acetate buffer (pH 3.50 - 8.00) were used as supporting electrolytes. Buffers and supporting electrolytes were prepared using CH_3COOH (100%), H_3PO_4 (Carlo Erba, 35%), and NaOH. Acetonitrile was used as the solvent for both pure water and organic environments. Potassium nitrate (KNO_3) and sodium chloride (NaCl) were used as supporting electrolytes in aqueous environment studies, while tetrabutylammonium tetrafluoroborate (TBATFB) salts were used in organic environment studies. Electrodes were polished using P2400 grit sandpaper followed by polishing with suspensions prepared using pure water and alumina powders of particle sizes 1 micron, 0.3 micron, and 0.05 micron. High purity nitrogen gas was used in the study.

Apparatus and instrumentation

The CHI660C model electrochemical analysis system was

used for voltammetric studies. Experiment solutions were analyzed using the Entek C-4 solid electrode working cell integrated into this system. A three-electrode design was employed in the experiments. Initially, a bare glassy carbon electrode was used as the working electrode, followed by a bismuth electrode obtained by coating this electrode with bismuth(III). An Ag/AgCl (saturated with KCl) electrode was used as the reference electrode, and a platinum wire served as the counter electrode. pH measurements were conducted using a PL-700PV pH meter. Deionized water used in preparing the solutions was obtained using a TKA Smart 2 Pure ultra-pure water system (conductivity of 0.055 µS/cm).

Procedure for preparing bismuth chloride solution

A 0.1 M stock solution of $Pb(NO_3)_2$ was prepared from a 0.1 M KNO_3 solution, and different concentrations of standard solutions were freshly prepared before each study. A coating solution of 100 ppm $BiCl_3$ was prepared. KNO_3 was used as the supporting electrolyte. The coating solution was prepared in an acetic acid/sodium acetate buffer environment.

A dopamine solution was prepared in 0.1 M H_2SO_4 with the presence of 10^{-3} M NaCl as the supporting electrolyte, while a ferrocene solution was prepared in acetonitrile with the presence of 0.1 M TBATFB as the supporting electrolyte.

Method

Alternating current voltammetry (CV), bulk electrolysis (BE), and SWASV techniques were employed in electrochemical studies. A glassy carbon electrode was coated with a bismuth film using amperometry technique at an appropriate potential. To characterize the developed bismuth electrode, the behaviors of the bare glassy carbon electrode and the modified electrode in the mediator medium were compared using cyclic voltammetry. Once it was determined that the electrode was modified, the behavior of lead on this surface was studied and compared with that on the bare glassy carbon electrode. Based on the high oxidation peak current and its dependence on concentration, anodic stripping voltammetry was employed for the determination process.

RESULTS AND DISCUSSION

Modifying the glassy carbon electrode

The behaviors of three different bare glassy carbon electrodes to be coated were examined in 10^{-3} M dopamine and 10^{-3} M ferrocene solutions. Differences in the peak changes in cyclic voltammetry were investigated. The accuracy of the working electrode to be modified was determined. The bare glassy carbon electrode was cleaned with sandpaper and polished with alumina powders of different sizes before each use. The glassy carbon electrode was coated with Bi(III) using the amperometry technique at a constant potential (-1 V) and used as the working electrode. A coating solution of 100 ppm $BiCl_3$ was prepared. The coating durations were tested at 300 s and 600 s.

As a result of the comparisons, it was observed that the reduction and oxidation peaks of the GC electrode coated for 300 seconds were not very regular. It was decided to continue the studies with 600 s coating.

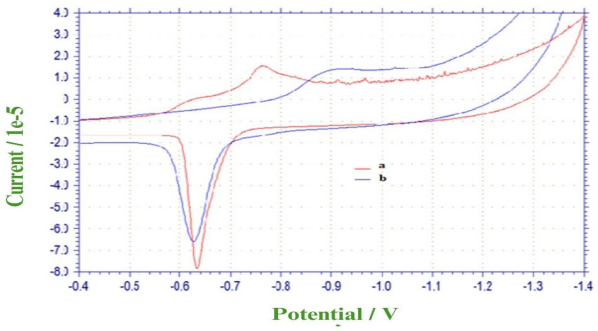

Figure 1. Comparison of cyclic voltammograms of GC electrodes coated with Bi(III) for (b) 300 s and (a) 600 s in 10^{-4} M Pb(II) solution

Electrochemical characterization of the bismuth-coated glassy carbon electrode in a 10^{-3} M dopamine solution

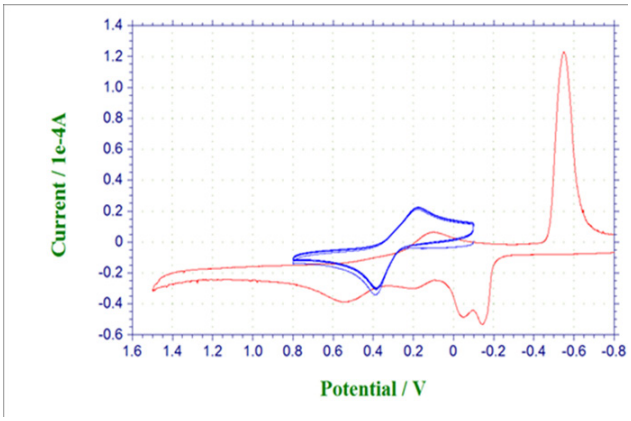

Figure 2. Simultaneous display of cyclic voltammograms obtained for a) Bi(III)-coated GC and b) bare GC immersed in 10^{-3} M dopamine solution (prepared in 0.1 M H_2SO_4 with 10^{-3} M NaCl supporting electrolyte), *v*= 100 mV/s (vs. Ag/AgCl).

When comparing the dopamine voltammograms obtained with the bare glassy carbon electrode and the bismuth-coated glassy carbon electrode, it is observed that the electrode has been successfully coated.

Electrochemical characterization of the bismuth-coated glassy carbon electrode in a 10^{-3} M ferrocene solution

When examining the behavior of ferrocene on bismuth-coated and bare glassy carbon electrodes, a shift in cathodic and anodic peak potentials was observed. Ferrocene is a mediator that undergoes rapid electron transfer. The change in peak separation on the two different surfaces indicates the presence of the coating.

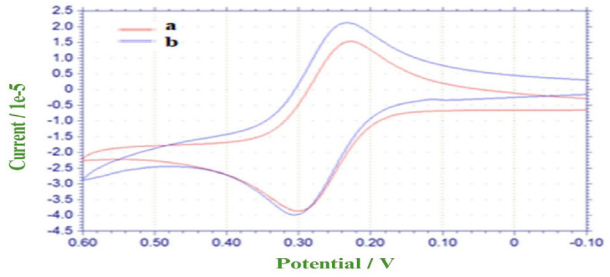

Figure 3. The combined appearance of cyclic voltammograms for (a) bare and (b) bismuth-coated GC immersed in a 10^{-3} M ferrocene solution (prepared in acetonitrile with 0.1 M TBATFB as the supporting electrolyte), v = 100 mV/s (vs. Ag/AgCl)

According to the obtained results, it has been understood that the peaks unrelated to dopamine arise from the oxidation of bismuth. The anodic peak at -0.2 V is attributed to the oxidation of bismuth.

With these results, when attempting to display the dopamine peak together with other peaks on the bare glassy carbon electrode, the situation depicted in Figure 4 below has emerged.

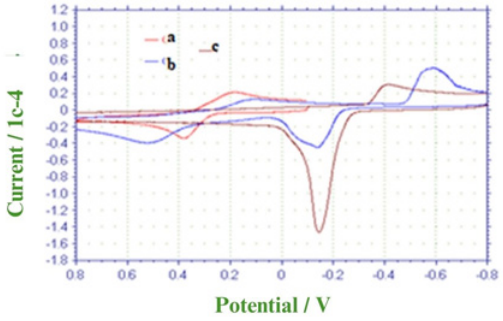

Figure 4. (a) Cyclic voltammograms obtained with a bare glassy carbon electrode and a bismuth-coated glassy carbon electrode in the presence of supporting electrolyte, (b) in environments with dopamine, (c) in environments without dopamine, *v* = 100 mV/s (vs. Ag/AgCl)

Based on the obtained results, it is understood that the anodic peaks are attributed to dopamine, while the other peaks not associated with dopamine are due to the oxidation and reduction of bismuth.

In these comparative experiments, the electrode was subjected to coating for 600 seconds. The same control was performed for bismuth behavior in an environment with and without ferrocene. In Figure 5, it is observed that the reduction and oxidation currents of ferrocene are larger on the bismuth-coated electrode. Additionally, no current was observed with the bismuth electrode in the presence of only the supporting electrolyte.

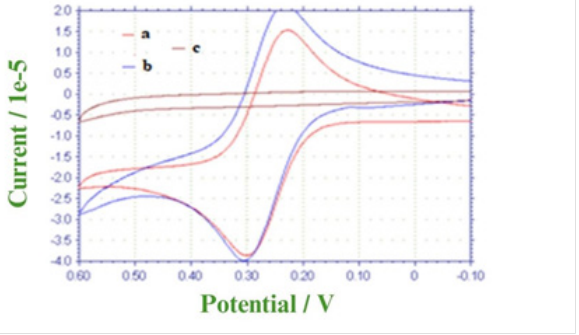

Figure 5. (a) Cyclic voltammograms obtained with the bare glassy carbon electrode and the bismuth-coated glassy carbon electrode in the presence of the supporting electrolyte, (b) in environments with ferrocene, and (c) in environments without ferrocene, v = 100 mV/s (vs. Ag/AgCl)

According to the obtained results, when comparing the bare glassy carbon electrode and the bismuth-modified electrode immersed in the ferrocene solution, it is observed that the anodic peaks belong to ferrocene, while the cathodic peaks at -0.2 V and -0.4 V correspond to the oxidation-reduction peaks of bismuth.

As seen in the figure, the peak separation in the cyclic voltammogram of ferrocene, which is a reversible system, has increased. This result indicates that the surface has been coated with bismuth. Moreover, the conductivity of the surface has not been significantly affected by this coating process.

The glassy carbon electrode was coated with Bi(III) using the Constant Potential Amperometry (i-t) technique. The surface was characterized using the Cyclic Voltammetry (CV) technique, confirming that the electrode was successfully coated. To explain the reduction and oxidation of lead ions on this electrode surface, as well as to perform deposition and stripping on the electrode surface, CV and SWASV electroanalytical techniques were used. The reduction and oxidation of Pb(II) ions on the prepared modified electrode surface were examined using the cyclic voltammetry technique. For the analytical determination of lead, deposition and stripping processes were applied using Square Wave Voltammetry with the optimization of necessary parameters.

Examination of lead (II) in bare GC electrode

Before coating, the reduction of lead on the bare glassy carbon electrode surface was examined in an aqueous medium. Nitrogen gas was passed through a 10^{-4} M $Pb(NO_3)_2$ solution for five minutes, and the cyclic voltammetry response was obtained. One reduction peak and one oxidation peak were observed. The observed peaks were identified as corresponding to lead (II) based on the cyclic voltammetry results obtained at different concentrations.

A $1x10^{-4}$ M $Pb(NO_3)_2$ solution was prepared from a 0.1 M stock solution in a 0.1 M KNO_3 supporting electrolyte medium. Initially, a CV experiment was conducted for the $1x10^{-4}$ M $Pb(NO_3)_2$ solution, and then 0.05 mL increments of the

stock $Pb(NO_3)_2$ solution were added to this analysis sample. The changes in voltammetric measurement results were monitored.

Investigation of Lead on the Bismuth-Coated Electrode

In this section of the experimental studies, following the bismuth coating procedure, the electrochemical behavior of lead on this surface was investigated. The same CV experiments conducted for Lead (II) on the bare GC electrode were repeated on the modified bismuth electrode surface. The experimental results obtained are presented in graph form in Figure 6.

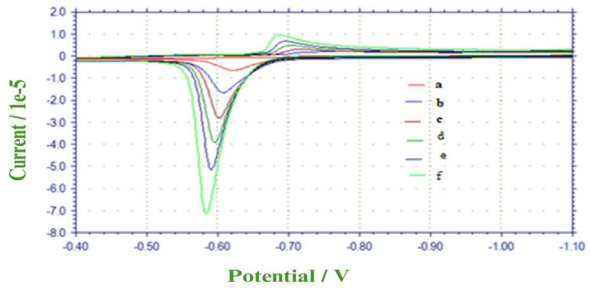

Figure 6. In the presence of a supporting electrolyte and 10^{-4} M Pb(II), cyclic voltammograms were obtained with (a) the bismuth-coated GC electrode in the same experimental cell, with additions of stock $Pb(NO_3)_2$ solution of (b) 0.05 mL, (c) 0.10 mL, (d) 0.15 mL, (e) 0.20 mL, and (f) 0.30 mL, *v*= 100 mV/s (vs. Ag/AgCl)

Analyses of the reduction of Pb(II) ions on the surface of the modified bismuth-coated electrode were conducted in the range of 0.1 µM to 1 µM. When the obtained reduction peaks were superimposed, it was confirmed that this signal belonged to Pb(II).

As observed in the study, on the surface of the modified GC electrode, a cathodic peak around -0.750 V and both cathodic and anodic peaks around -0.600 V were detected. Accordingly, the difference between the cathodic and anodic peak potentials is approximately 50 mV, which is consistent with Nernstian behavior.

SWASV Optimization on Bi(III)-Coated Electrode

The coating durations necessary for preparing the bismuth electrode were tested for 300 s and 600 s. Based on this comparison, the 600 s coating duration was preferred due to the smaller difference between the cathodic and anodic peak potentials and the higher peak intensities.
Comparisons revealed that the reduction and oxidation peaks of the GC electrode coated for 300 seconds were not very regular. Therefore, it was decided to continue the experiments with a 600-second coating.

Square Wave Anodic Stripping Voltammetry (SWASV) Results

Upon examining the lead peaks recorded by cyclic voltammetry, it was observed that the oxidation peaks were sharper and there were more significant increases in the anodic current with increasing concentration. Therefore, a method development involving accumulation and stripping using SWASV technique was decided. Experimental parameters for SWASV were investigated. The effects of Pb(II) accumulation time (t_{acc}), accumulation potential (E_{acc}), and accumulation frequency (f_{acc}) on peak height were studied and optimized in the modified electrode. These parameters' impact on peak height in SWASV studies was examined. After determining the experimental parameters, the effect of increasing Pb(II) concentration on peak height was investigated.

Optimization of Accumulation Time

In the study, using a modified electrode with a 600-second coating time in 10^{-5} M $Pb(NO_3)_2$ solution, cyclic voltammograms were taken to optimize the accumulation time, which was explored at intervals of 30, 60, 90, 120, 150, 210, 240, and 270 seconds. Considering the need for increased peak height without compromising peak symmetry, an accumulation time of 210 s was determined.

Table 1. Current values at different accumulation times obtained from 10^{-5} M Pb(II) in SWSV (currents are the average of three measurements)

Current (ip) x 10^{-4}	Accululation Time (s)
0.437	30
1.252	60
1.532	90
1.711	120
1.883	150
2.059	210
2.183	240
2.346	270

Optimization of accumulation frequency (f)

To optimize the frequency, one of the parameters of square wave voltammetry, square wave voltammograms were compared at 14 different frequencies starting from 15 Hz and increasing by 15 Hz increments, using a 210 s accumulation time with a 10^{-5} M $Pb(NO_3)_2$ solution. It was determined that the optimal frequency where the peak shape remained undistorted was 15 Hz. At other frequencies, although peak currents increased, peak shapes became distorted and broadened. These characteristics rendered the peaks unsuitable for quantitative purposes, thus they were not preferred.

Optimization of Accumulation Potential

With an accumulation time of 210 s and a frequency of 15 Hz, the optimization of accumulation potential was conducted at -0.7, -0.8, -0.9, and -1.0 V. Upon comparing these four different potentials, it was determined that the optimal accumulation potential is -0.8 V.

Table 2. SWASV results of current values at different accumulation potentials obtained from 10^{-5} M Pb(II) (currents are averages of two measurements)

Current (ip) x 10^{-4}	Accumulation Potential (V)
0.032	-0,7
2.059	-0,8
1.090	-0,9
1.047	-1

Determining the Analytical Working Range

After optimizing the necessary parameters, the concentration-current relationship for lead was investigated under these conditions. According to the optimization studies, the accumulation potential was set at -0.8 V, accumulation time at 210 s, and frequency at 15 Hz. Current values were plotted in the range of 0.1-1 µM concentration.

Table 3. Under optimum conditions, current values obtained at different concentrations (standard deviations calculated from three measurements)

Concentration, µM	Current, 10^{-5} A
1	1.372±0.02
0.8	1.142±0.05
0.6	0.794±0.03
0.4	0.392±0.04
0.2	0.109±0.02
0.1	0.03±0.01

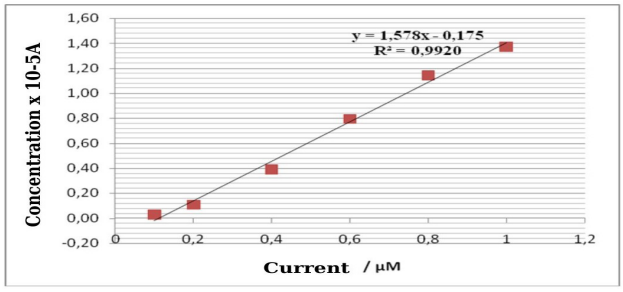

Figure 7. Calibration curve obtained at different concentrations for Pb(II) ion using bismuth-coated GC electrode under optimum conditions. Standard $Pb(NO_3)_2$ concentrations: 0.1 µM, 0.2 µM, 0.4 µM, 0.6 µM, 0.8 µM, and 1 µM.

Table 4. Analytical determination parameters according to the working graph obtained in the range of 0.1-1 µM (pH = 4.50) in 0.2 M acetate buffer

Parameters	Results
Concentration Range (µM)	0.1 – 1
Slope 10^{-5}A μM^{-1}	1.578
Standard Deviation of Slope (S_m)	0.099
Correlation Coefficient, r	0.996
Regression Standard Deviation, s_r	0.057
Number of Measurements, n	3
Detection Limit, LOD(M)	3.3 x 10^{-9}
Lower Detection Limit, LOQ(M)	1.1 x 10^{-8}

Upon examination of Figure 7 and Table 4, the optimal linear range was determined to be 0.1 µM-1 µM.

Calculation of LOD (limit of detection) and LOQ (limit of quantification)

By measuring at the lowest detectable concentration of 1x10^{-8} M, the average and standard deviation were calculated. The LOD value was determined as 3xS/m and the LOQ value as 10xS/m using the formula specified in Table 4 (Skoog, 2004).

Voltametric determination and recovery of lead(II) in sugar beet wash water using a bismuth-modified electrode

A mixture was prepared by taking 50 mL of sugar beet wash water as the sample and 50 mL of 0.2 M KNO_3 solution as the supporting electrolyte. Separate cells were used for each set of three measurements taken. The measured current values were substituted into the calibration graph equation obtained as y=1.78×-0.175 to calculate the amount of lead(II).

For recovery, a concentration of 2×10^{-6} M of 10^{-4} M $Pb(NO_3)_2$ solution was added to wastewater sample containing 1.6×10^{-7} M Pb(II). Three separate cells were prepared, and three measurements were taken in each cell. The amount of lead(II) corresponding to the added Pb(II) substance was calculated in milligrams based on the obtained current value. The recovery of the wastewater sample was calculated as 97.5% by comparing the added lead(II) amount with the found lead(II) amount.

Table 5. Measurement of lead(II) amount in wastewater sample and recovery of lead

Parameters	Results
Relative standard deviation (%R.S.D)	2.344
Added	4.144×10^{-3} mg
Found	8.84×10^{-3} mg
Recovery (%)	97.5

Table 6. Comparison of analytical performance measurements of bismuth coated GC with different modified electrodes in the literature for the determination of heavy metal ions.

Electrode	Technique	LOD	Ref.
N^1-hydroxy-N^1,N^2-diphenylbenzamidine-Carbon paste electrode(CPE)	ASWSV	0.0094 nM (Pb)	(29)
(Ag)/ (Au)-(NP)glassy carbon electrode(GCE)	DPASV	0.03×10^{-2} µg /L (Pb)	(30)
Bi oxycarbide /GCE	DPASV	3.97 µg /L (Pb)	(31)
Bi/carboxyphenyl-modified GCE	ASWSV	10 µg /L (Pb)	(32)
Graphene quantum dots and Nafion modified GCE	ASWSV	8.49 µg /L (Pb)	(33)
BE-MCPE	DPASV	4.89×10^{-8} M	(34)
Bismuth coated GC	ASWSV	3.3×10^{-9} M	This work

It is shown in Table 6 that the Bismuth coated GC exhibits good sensitivity and selectivity for the detection of Pb(II). It can be said that it is an electrode that can be used for trace amounts of lead analysis. Table 6 also compares the analytical performance measurements of the Bismuth coated GC with other modified electrodes reported in the literature. When compared with the literature, it is seen that a very suitable LOD value for Pb^{+2} detection of bismuth-coated GC is achieved. In addition, this electrode can be prepared quickly and is cost-effective.

CONCLUSION

In this study, a method was first developed for the electrochemical determination of Pb(II) ions using SWASV on a bismuth-coated glassy carbon electrode. The developed method was then applied to a sugar beet washing water sample. The current value obtained for the sample was substituted into the calibration equation to determine the amount of Pb(II).

The working concentration range of the developed method was determined to be 0.1 µM – 1 µM. Since no current reading can be obtained for control solutions without any electroactive species in electrochemical determination methods, the lower detection limit was determined as 0.01 µM, which is the lower limit of the working range and the smallest concentration at which a current reading can be made.

In the analytical application of this method, the amount of Pb(II) in the sugar beet washing water sample taken from Çorum Sugar Factory was found to be (0.16±0.09) µM. Measurements were taken for three different samples, and the standard deviation value was calculated using these three measurements. The amount of Pb in the washing water sample corresponds to 0.03 ppm. This value is below the highest level of 0.14 ppm that can be found in industrial waters or nearby areas (Gündüz, 1998).
As seen in Table 5, the recovery rate was found to be 97.5%, leading to the conclusion that the presence of Pb(II) does not interfere with our method.

According to the simultaneous results obtained from an external laboratory for the sugar beet washing water sample taken from Çorum Sugar Factory, the amount of Pb(II) was determined to be '< 0.04 µM'.

Voltammetric stripping techniques are used for the determination of trace amounts of substances in aqueous and non-aqueous environments. Along with atomic absorption, neutron activation, fluorometric, and chromatographic methods, voltammetric stripping methods are considered among the five important methods used in trace analysis. Among these methods, the two most widely used in inorganic analysis are atomic absorption and stripping methods. While atomic absorption is only used for inorganic determinations, stripping techniques can be used for both inorganic and organic determinations. Additionally, atomic absorption is a destructive method, whereas stripping methods are non-destructive. The equipment used in stripping techniques is simpler and cheaper. The same sample can be analyzed multiple times using stripping techniques.

In conclusion, an effective method has been developed for the rapid, easy application, low cost, and low detection limit determination of lead ions, one of the heavy metals found in the wash waters resulting as waste in the production process of sugar factories.

Sugar beet processing water is the waste of water used in the process of obtaining sugar from beet along with dissolved organic and inorganic substances. This wastewater contains a variety of components and can have environmental impacts. Process water contains various substances such as sugar, acids, organic substances, nitrogen and phosphorus components. With appropriate treatment processes, process water can be reused in various fields, such as irrigation in agriculture or energy production. It is important to manage and treat wastewater in accordance with environmental protection laws. As a result, it can be said that sugar beet processing water wastes may cause environmental problems if not managed correctly. Therefore, studies should be carried out to develop treatment methods and keep waste under control**.**

ACKNOWLEDGEMENT

We would like to thank Hitit University Scientific Research Projects Coordination Office for their support to this study within the scope of project number FEF03.13.003.

REFERENCES

1. Mohamed A, Sheikka MA. Spectrophotometric determination of clozapine based on its oxidation with bromate in a micellar medium. IL Farmaco, 59 (2004) 907. DOI: 10.1016/j.farmac.2004.07.008.
2. Hammam E, Tawfik A, Ghoneim AA. Adsorptive stripping voltammetric quantification of the antipsychotic drug clozapine in bulk form, pharmaceutical formulation and human serum at a mercury electrode. Journal of Pharmaceutical Biomedical Analysis 36 (2004) 149. DOI: 10.1016/j.jpba.2004.04.012.
3. Güven FM, Birsöz S. Klozapin ve Şizofreni Sağaltımındaki Yeri.

Klinik Psikiyatri 4 (2001) 124-128.
4. Lieberman JA, Saltz BL, Johns CA, Pollack S, Borenstein M, Kane J. The effects of clozapine on tardive dyskinesia. The British Journal of Psychiatry 158 (1991) 503. DOI: 10.1192/bjp.158.4.503.
5. Freudenreich O, Henderson DC, Walsh JP, Culhane M.A., Goff DC. Risperidone augmentation for schizophrenia partially responsive to clozapine: A double-blind, placebo-contolled trial. Schizophrenia Research 92 (2007) 90. DOI: 10.1016/j.schres.2006.12.030
6. Guitton C, Kinowski JM, Regis A., Bressolle F. Determination of clozapine and its major metabolites in human plasma and red blood cells by high-performance liquid chromatography with ultraviolet absorbance detection. Journal of Chromatography B 690 (1997) 211-222. DOI: 10.1016/S0378-4347(96)00362-3.
7. Taha EA, Soliman SM, Abdellatef HE, Ayad MM. Colorimetric methods for the determination of some tricyclic antidepressant drugs in their pure and dosage forms, Mikrochimica Acta 140 (2002) 175-182. DOI:10.1007/s00604-002-0904.
8. Gosser Jr. DK, Cyclic Voltammetry: Simulation and analysis of reaction mechanisms, VCH Publishers, New York, 1983, ISBN: 978-1560810261.
9. Mashhadizadeh MH, Afshar E. Electrochemical investigation of clozapine at TiO_2 nanoparticles modified carbon paste electrode and simultaneous adsorptive voltammetric determination of two antipsychotic drugs. Electrochimica Acta 87 (2013) 816. DOI: 10.4103/2229-5186.79345.
10. Weber JM, Volke J. 75 years in the polarography of pharmaceuticals and physiologically active substances. Pharmazie 46 (1991) 853.
11. Edno L, Combourieu I, Cazenave M, Tignol J. Assay for quantitation of clozapine and its metabolite N-desmethyl clozapine in human plasma by high performance liquid chromatography with ultraviolet detection. Journal of Pharmaceutical and Biomedical Analysis 16 (1997) 311. DOI: 10.1016/s0731-7085(97)00048-4.
12. Raggi MA, Bugamelli F, Mandrioli R, Sabbioni C, Volterra V, Fanali S. Rapid capillary electrophoretic method for the determination of clozapine and desmethylclozapine in human plasma, Journal of Chromatography A 916 (2001) 289-296. DOI: 10.1016/S0021-9673(01)00520-9.
13. Elqudaby HM, Mohamed GG, El-Din GMG. Electrochemical behaviour of trimebutine at activated glassy carbon electrode and its direct determination in ürine and pharmaceutics by square wave and differential pulse voltammetry. International Journal of Electrochemical Science 9 (2014) 856-869.
14. Demirbilek E, Saglıkoglu G, Yılmaz S. Electrochemical investigation of isoniazid on poly (p-aminobenzene sulfonic acid) film modified glassy carbon electrode. International Journal of Electrochemical Science 10 (2015) 4428-4438.
15. Shahrokhian S, Kamalzadeh Z, Hamzehloei A. Electrochemical determination of clozapine on MWCNTs/New coccine doped PPY modified GCE: An experimental design approach, Bioelectrochemistry 90 (2013) 36. DOI: 10.1016/j.bioelechem.2012.10.002.
16. Tammari E, Neshadali A, Lotfi S, Veisi H. Fabrication of an electrochemical sensor based on magnetic nanocomposite Fe3O4/β-Alanine/Pd modified glassy carbon electrode for determination of the nanomolar level of clozapine in biological model and pharmaceutical samples. Sensors and Actuators B: Chemistry 241 (2017) 879. DOI: 10.1016/j.snb.2016.11.014.
17. Gökmeşe F, Gökmeşe E, Emire Z. A simple and rapid method for preparing carbon nanopore electrode ensemble coating a glassy carbon electrode with chromate. Hittite Journal of Science and Engineering 3 (2016) 1. DOI: 10.17350/HJSE19030000025.
18. Bard AJ, Faulkner LR. Electrochemical Methods; Fundamentals and Applications. John Wiley and Sons, Inc., New York, 2001, ISBN: 0-471-04372-9, page 833.
19. Shrivastava A., Gupta VB. Methods for the determination of limit of detection and limit of quantitation of the analytical methods. Chronicles of Young Scientists 2 (2011) 21. DOI: 10.4103/2229-5186.79345.
20. K. Farhadi, A. Karimpour, Electrochemical behavior and determination of clozapine on a glassy carbon electrode modified by electrochemical oxidation, Anal. Sci. 23, (2007) 479.
21. N.P. Shetti, D.S. Nayak, S.J. Malode, R.M. Kulkarni, An electrochemical sensor for clozapine at ruthenium doped TiO_2 nanoparticles modified electrode, Sensors and Actuators B: Chem.
22. Yavaş, A., N., 2014. Karbon Pasta Elektrotların Bitki Dokuları ile Modifikasyonu ve Elektrokataliz Özelliklerin İncelenmesi. Yüksek Lisans Tezi, Adnan Menderes Üniversitesi, Fen Bilimleri Ensitüsü, Aydın. Y7 (2017) 858.
23. Hutton, E.A., Hocevar, S.B., Ogorevc, B., 2004. Ex Situ Preparation of Bismuth Film Microelectrode For Use In Electrochemical Stripping Microanalysis. Analytica Chimica Acta, 537, 285-292.
24. Economou, A., Fielden, P.R., 2005. Bismuth-film elecrodes:recent developments and potentialities for electroanalysis. Trends in Analytical Chemistry, Vol. 24, No. 4, 334-339.
25. Wang, J. 2000. Analytical Electrochemistry. 2nd edition. John Wiley and Sons. Inc. New York.
26. Kristie, C.A., Tatum, C.E., Dansby-Sparks, R.N., Chambers, J.Q., Xue, Z., 2010. Individual and Simultaneous Determination of Lead, Cadmium, and Zinc by Anodic Stripping Voltammetry at a Bismuth Bulk Electrode. Talanta, 82, 675-680.
27. Burç, M., Duran, S.T., Güngör, Ö., Karagözler, A.E.,2024. Determination of gentamicin by using square wave anodic stripping voltammetry with poly (β-cyclodextrin-p-toluene sulfonic acid) modified glassy carbon electrode. Polymer Bulletin, 81, 6381–6403.
28. Dahaghin, Z., Kilmartin, P.A., Mousavi, H.Z., 2020. Novel ion imprinted polymer electrochemical sensor for the selective detection of lead(II). Food Chemistry, 303, 125374.
29. Tesfaye E, Chandravanshi BS, Negash N, Tessema M., 2022. A new modified carbon paste electrode using N1-hydroxy-N1,N2-diphenylbenzamidine for the square wave anodic stripping voltammetric determination of Pb(II) in environmental samples. Sens Bio-Sensing Res. 100520.
30. Yadav R, Berlina AN, Zherdev A V., Gaur MS, Dzantiev BB., 2020. Rapid and selective electrochemical detection of Pb^{2+} ions using aptamer-conjugated alloy nanoparticles. SN Appl Sci vol. 2:2077.
31. Zhang Y, Li C, Su Y, Mu W, Han X., 2020. Simultaneous detection of trace Cd(II) and Pb(II) by differential pulse anodic stripping voltammetry using a bismuth oxycarbide/nafion electrode. Inorg Chem Commun. 111:107672.
32. Phal S, Nguyễn H, Berisha A, Tesfalidet S., 2020. In situ Bi/carboxyphenyl-modified glassy carbon electrode as a sensor platform for detection of Cd^{2+} and Pb^{2+} using square wave anodic stripping voltammetry. Sens Bio-Sensing Res.;34:100455.
33. Pizarro J, Segura R, Tapia D, Navarro F, Fuenzalida F, Jesús Aguirre M., 2020. Inexpensive and green electrochemical sensor for the determination of Cd(II) and Pb(II) by square wave anodic stripping voltammetry in bivalve mollusks. Food Chem. 321:126682.34
34. Tüzün E., 2023. Voltammetric Determination of Trace Amounts of Lead with Novel Graphite/Bleaching Earth Modified Electrode. Journal of the Turkish Chemical Society Chemistry, 10(3) 659-670.

HİTİT JOURNAL OF SCIENCE

e-ISSN: 3061-9629
Volume: 2 • Number: 1
January 2025

Synthesis, Structural Characterization, and Thermal Stability Investigation of Methoxybenzamide Derivatives Containing the 5-Mercapto-1,3,4-Thiadiazol-2-yl Group

Şenol YAVUZ[1,*] | Ersin Demir[2] | Naki ÇOLAK[3] | Dursun Ali KÖSE[3]

[1]Department of Property Protection and Security, Osmancık Ömer Derindere Vocational School, Hitit University, 19500, Corum, Türkiye.
[2]Amasya University, Central Research Laboratory, 05100 Amasya, Türkiye.
[3]Department of Chemistry, Science & Arts Faculty, Hitit University, 19000, Corum, Türkiye.

Corresponding Author

Şenol YAVUZ
E-mail: senolyavuz@hitit.edu.tr Phone: +90 535 213 6271
RORID: ror.org/01x8m3269

Article Information

Article Type: Research Article
Doi: -
Received: 10.01.2025
Accepted: 22.01.2025
Published: 31.01.2025

Cite As

Yavuz S., et al. Synthesis, Structural Characterization, and Thermal Stability Investigation of Methoxybenzamide Derivatives Containing the 5-Mercapto-1,3,4-Thiadiazol-2-yl Group. 2025;2(1):18-25.

Peer Review: Evaluated by independent reviewers working in at least two different institutions appointed by the field editor.
Ethical Statement: Not available.
Plagiarism Checks: Yes - iThenticate
Conflict of Interest: The authors have no conflicts of interest to declare.

CRedit Author Statement
Şenol YAVUZ: Design of the study, writing, reviewing, editing, supervisio
Ersin DEMİR: Planning of the syntheses, writing of the article, experimental procedure.
Naki ÇOLAK: The experimental procedure, NMR and LC/MS analysis, and structural characterization.
Dursun Ali KÖSE: The investigation of the thermal stability of derivatives and their elemental analysis, writing of the article.

Synthesis, Structural Characterization, and Thermal Stability Investigation of Methoxybenzamide Derivatives Containing the 5-Mercapto-1,3,4-Thiadiazol-2-yl Group

Şenol YAVUZ1,* | Ersin Demir2 | Naki ÇOLAK3 | Dursun Ali KÖSE3
[1]Department of Property Protection and Security, Osmancık Ömer Derindere Vocational School, Hitit University, 19500, Corum, Türkiye.
[2]Amasya University, Central Research Laboratory, 05100 Amasya, Türkiye.
[3]Department of Chemistry, Science & Arts Faculty, Hitit University, 19000, Corum, Türkiye.

Abstract
Compounds with a methoxy benzamide structure contain a methoxy group (–OCH_3) and an amide functional group (–$CONH_2$) within a benzene ring. This causes the compound to exhibit a complex structure with polar and nonpolar characteristics. These compounds are significant in pharmaceutical chemistry, biological research, and chemical synthesis. Due to its active properties, the "N–C–S" linkage in the thiadiazole ring can chelate metal ions. The antimicrobial activity of benzamide compounds derived from thiazoles and their wide applications in medicine increases the importance of methoxybenzamide derivatives. In this study, 5-amino-1,3,4-thiadiazole-2-thiol compounds were reacted with 2-methoxy, 3-methoxy, and 4-methoxybenzoyl chloride in toluene under a reflux condenser, resulting in the synthesis of methoxybenzamide derivatives (a, b, c). The structural characterization of the obtained methoxybenzamide (a, b, c) compounds was performed using FTIR, LC/MS-ESI, 1H NMR, 13C APT spectroscopy, and elemental analysis. Additionally, the thermal stability of the synthesized methoxybenzamide compounds was investigated through thermal analysis (TGA/DTA/DTG).

Keywords: Methoxybenzamide, 1,3,4-thiadiazol, Synthesis, Structural Characterization, Thermal Stability,

INTRODUCTION
Nonlinear optical materials containing amides play a significant role in the evolution of modern technology (Figure 1). These compounds notably impact technology and industrial applications [1-5]. Recent studies in nonlinear optics have highlighted the significant potential of second-order organic optical materials. These materials are recognized for their versatility and effectiveness across a range of applications, including photonics, which involves the generation, manipulation, and detection of photons; lasers, where they serve as crucial components for light amplification; and electro-optic switches, which enable rapid control of light signals in communication systems. Additionally, second-order organic materials play a vital role in frequency conversion processes that allow for the generation of new wavelengths of light, essential for telecommunications and data transmission. Their unique properties also make them suitable for advanced data storage solutions, improving the efficiency and capacity of information technology systems. [6-9].

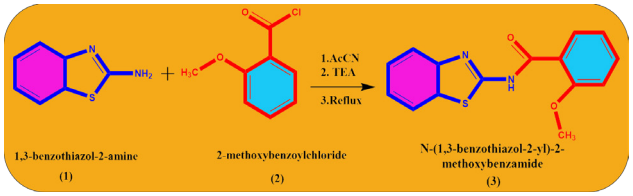

Figure 1. Synthesis of a compound containing methoxybenzamide [4].

Pyrazole is a five-membered ring compound containing two adjacent nitrogen atoms [10,11]. Knorr's 1883 discovery of antipyrine inspired the chemical structure of pyrazole. Since that time, numerous new derivatives have been synthesized. The pyrazole derivative compounds obtained have been found to exhibit a wide range of biological activities, including anticancer [12], anti-inflammatory [13], analgesic [14], antihypertensive [15], antipyretic [16], antimicrobial [17], and antioxidant [18] properties [19]. Among the drugs available on the market, Sildenafil, Celebrex, Zometapin, Fipronil, Rimonabant, and Lonazolac show therapeutic potential [20]. 1,3,4-Thiadiazoles are a crucial class of heterocyclic compounds. The "N–C–S" linkage in 1,3,4-thiadiazole can serve as an active site, demonstrate good tissue permeability, and chelate various metal ions in the body. The aromaticity of thiadiazole significantly influences its lower toxicity and in vivo stability [21]. So far, thiadiazoles have demonstrated impressive antiviral [22], antimicrobial [23], anti-inflammatory [24], antituberculosis [25], and anticancer [26] activities. 1,3,4-Thiadiazole is also found in many drugs, such as ceftazidime, cefazolin, acetazolamide, methazolamide, and megazol [27]. Amid derivatives are widely used in medicinal chemistry, organic compounds, and biomolecules due to the prevalence of amide bonds and their biological activity in living systems [28-31].

To discover and design more effective and cost-efficient drugs for clinical use, hybrid molecules have been created by combining different pharmacophores through a thorough literature review. This approach aims to achieve synergistic chemotherapeutic activity, increased selectivity, and minimized toxicity. As a result, pyrazole-containing thiazole [32], 1,2,4-oxadiazole [33], 1,3,4-oxadiazole [34], 1,2,4-triazoles, and benzoxazoles [35] have been synthesized, and an increase in pharmacological activity has been observed. Additionally, many biologically active pyrazolyl-1,3,4-thiadiazole derivative compounds have been synthesized. Therefore, studies on synthesizing pyrazole-based thiadiazole derivatives have gained importance [36,37].

Problems arise due to the increasing resistance to drugs during the treatment of fungal infections [38-42]. Therefore, the results obtained when synthesizing new antifungal compounds indicate that tetrazole-containing compounds provide more effective outcomes. These azole compounds inhibit the growth of many pathogenic strains. For example, 1-(2,4-dihydroxythiobenzoyl) tetrazoles and tetrazole compounds containing hydrazone groups exhibit high antifungal activity against Candida spp. [43-46]. Tetrazole-based compounds, distinguished by the presence of both hydrazone and thiazoline functional groups, have demonstrated notable antifungal properties. These compounds are particularly effective against a range

of fungal pathogens, including Trichoderma harzianum, Aspergillus ochraceus, and several species of Fusarium such as Fusarium solani, Fusarium moniliforme, and Fusarium culmorum. Additionally, they have shown activity against Candida albicans, making them promising candidates for the development of antifungal treatments [47]. Tetrazoles with a quinolone scaffold are effective against C. albicans and A. niger, while tetrazole derivatives with triazine dendrimeric chalcones show high fungicidal activity against C. albicans, A. niger, A. fumigatus, and Saccharomyces cerevisiae [48-52].

EXPERIMENTAL

Reagents and Instrumentation

All melting points are uncorrected and in °C with a Gallenkamp apparatus. FT-IR spectra were recorded on a Thermo Nicolet 6700 Spectrometer (ATR). NMR spectrometer and chemical shifts are expressed in 6 ppm using TMS as an internal standard. using a Bruker AVANCE III spectrometer. Mass spectra were obtained (LC-MS/MS) method with a Thermo Scientific / TSQ Quantum Access Max Mass Spectrometer. Compounds were thermally analyzed using a Shimadzu DTG-60 and a Perkin Elmer Pyris TGA device. Elemental analyses were conducted using the Leco TruSpec Micro Elemental Device.

General synthesis of N-(5-mercapto-1,3,4-thiadiazol-2-yl)-2/3/4-methoxybenzamide (a-c)

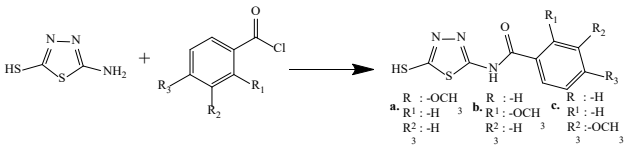

Figure 2. General synthetic procedure of methoxybenzamide derivatives (a-c)

Substances *5-amino-1,3,4-thiadiazole-2-thiol* (1.33 g, 1.0 mmol) and pyridine (1.0 mmol) were placed in toluene (5 mL) a balloon in which nitrogen gas was passed. 2-methoxybenzoyl chloride (a, b, c) was added to this mixture drop by drop within 10 minutes. The mixture was boiled under the back cooler until the reaction was complete. The completion of the reaction was checked by TLC (n-hexane: ethyl acetate, 1:1). After 4 hours, the reaction was completed, and pyridine was extracted with water (3 times 15 mL). Toluene was evaporated under reduced pressure. The resulting precipitate was crystallized in ethanol [53,54].

N-(5-mercapto-1,3,4-thiadiazol-2-yl)-2-methoxybenzamide, (a).

As stated in headline 2.2, it was prepared based on items 5-amino-1,3,4-thiadiazole-2-thiol and 2-methoxybenzoyl chloride. Yield: 0.60 g (75%); white solid. Melting point: 246-247 °C; FT-IR (ATR, cm^{-1}) : 3271 NH, 3124, 3082 aromatic C-H, 2981, 2936, 2835 aliphatic C-H, 1648 CO, 1595 C=C. ^{1}H NMR spectra data (ppm, d_6-DMSO): 7.63-7.61 (d, 1H, Ar-H), 7.53-7.49 (t, 1H, j=7.46 Hz, Ar-H), 7.14-7.11 (d, 1H, Ar-H), 7.01-6.99 (t, 1H, j=7.46 Hz, Ar-H), 3.81 (s, 3H, OCH_3). ^{13}C NMR APT (ppm, d_6-DMSO): Negative amplitude: 167.82 (HS-C), 159.35 (C=O), 158.48 (Ar-C-OCH_3), 157.69 (S-C=N), 121.69 (Ar-C-CO). Positive amplitude: 133.51 (Ar-CH), 131.07 (Ar-CH), 120.47 (Ar-CH), 112.71 (Ar-CH), 56.14 (OCH_3). MS (-ESI): m/z 265.99 ([M-H]$^-$; $C_{10}H_9N_3O_2S_2$ (M=267.32 g/mol).

N-(5-mercapto-1,3,4-thiadiazol-2-yl)-2-methoxybenzamide, (b).

As stated in headline 2.2, it was prepared based on items 5-amino-1,3,4-thiadiazole-2-thiol and 3-methoxybenzoyl chloride. Yield :0.48 g (60%); white solid. Melting point: 245-247 °C; FT-IR (ATR, cm^{-1}) : 3215 NH, 3086 aromatic C-H, 2942, 2847, 2821 aliphatic C-H, 1676, 1642 CO, 1577 C=C. ^{1}H NMR spectra data (ppm, d_6-DMSO): 8.79 (s, 1H, NH), 7.71 (s, 1H, Ar-H), 7.54-7.52 (s, 1H, Ar-H), 7.44-7.42-7.40 (t, 1H, Ar-H), 7.21-7.20-7.19 (d, 1H, Ar-H), 3.86 (s, 3H, OCH_3). ^{13}C NMR APT (ppm, d_6-DMSO): Negative amplitude: 172.75 (HS-C), 167.57 (C=O), 162.84 (Ar-C-OCH_3), 159.75 (S-C=N), 132.71 (Ar-C-CO). Positive amplitude: 130.16 (Ar-CH), 122.00 (Ar-CH), 119.33 (Ar-CH), 114.35 (Ar-CH), 55.93 (OCH_3). MS (-ESI): m/z 266.94 ([M-H]$^-$; $C_{10}H_9N_3O_2S_2$ (M=267.32 g/mol).

N-(5-mercapto-1,3,4-thiadiazol-2-yl)-2-methoxybenzamide, (c).

As started in headline 2.2, it was prepared the basis of items *5-amino-1,3,4-thiadiazole-2-thiol* and 4-methoxybenzoyl chloride. Yield : 0.57 g (71%); white solid. Melting point: 244-246 °C; FT-IR (ATR, cm^{-1}) : 3263 NH, 3057, 3017 aromatic C-H, 2898, 2849 aliphatic C-H, 1666, 1624 CO, 1593, 1565 CC. ^{1}H NMR spectra data (ppm, d_6-DMSO): 8.81 (s, 1H, NH) 7.91, 7.82 (d, 2H, Ar-H), 7.03-7.00 (d, 2H, Ar-H), 3.82 (s, 3H, OCH_3). ^{13}C NMR APT (ppm, DMSO-d_6) (The solvent peak was referenced when giving the APT. The solvent peak here is located on the opposite side compared to the others): Positive amplitude: 172.53 (HS-C), 167.48 (C=O), 163.27 (Ar-C-OCH_3), 123.39 (Ar-CH). Negative amplitude: 131.80 (Ar-CH), 114.51 (Ar-CH), 56.06 (OCH_3). MS (-ESI): m/z 266.93 ([M-H]$^-$; $C_{10}H_9N_3O_2S_2$ (M=267.32 g/mol).

RESULT AND DISCUSSION

Elemental Analysis

CHNS elemental analyses of molecules were performed and when the obtained results were examined, it was determined that the experimental and theoretical element composition percentages were compatible. The values in parentheses were calculated theoretically, while the others are the experimentally found percentage compositions.

N-(5-mercapto-1,3,4-thiadiazol-2-yl)-*2*-methoxybenzamide (a):

C: 44.52% (44.93%); H: 4.12% (3.39%); N: 15.87% (15.72%); S: 23.65% (23.99%)

N-(5-mercapto-1,3,4-thiadiazol-2-yl)-*3*-methoxybenzamide (b):

C: 44.15% (44.93%); H: 4.21% (3.39%); N: 15.63% (15.72%); S: 23.71% (23.99%)

N-(5-mercapto-1,3,4-thiadiazol-2-yl)-*4*-methoxybenzamide (c):

C: 44.33% (44.93%); H: 4.05% (3.39%); N: 15.58% (15.72%); S: 23.81% (23.99%)

FTIR Analysis

Methoxybenzamide derivatives (a, b, c) were obtained from the reaction of 5-amino-1,3,4-thiadiazole-2-thiol with methoxybenzamide compounds (2-methoxy, 3-methoxy, 4-methoxy). FTIR spectroscopy was initially used to characterize the structure of the obtained compounds. In the starting compound, 5-amino-1,3,4-thiadiazole-2-thiol, the -NH_2 group shows a broad stretching band around 3400 cm^{-1}

in the FTIR spectrum. In the synthesized methoxybenzamide compounds, a weak stretching band around 3263 cm^{-1} is observed, indicating the formation of the amide bond and confirming that the reaction has occurred. The C=O stretching bands in the structures of the a, b, and c methoxybenzamide compounds are close at 1648, 1642, and 1624 cm^{-1}, respectively, demonstrating that the obtained compounds are correct.

^{13}C NMR APT and ^{1}H NMR Analysis

In the ^{1}H NMR spectrum of N-(5-mercapto-1,3,4-thiadiazol-2-yl)-2-methoxybenzamide (a), chemical shifts correspond to four different protons in the aromatic region. In the 1H NMR spectrum of N-(5-mercapto-1,3,4-thiadiazol-2-yl)-3-methoxybenzamide (b), five different proton chemical shifts are observed in the aromatic region, while in N-(5-mercapto-1,3,4-thiadiazol-2-yl)-4-methoxybenzamide (c), due to the para position of the methoxy group on the benzene ring, the protons in the benzene ring are symmetric, and two different proton chemical shifts are observed. The different chemical shifts of the aromatic protons indicate that the three compounds are distinct. In compounds b and c, a singlet for the N-H group chemical shift is observed at 8.79 and 8.81, while no chemical shift for the N-H group is observed in compound a. ^{1}H and ^{13}C NMR spectra of the synthesized new compounds were recorded in Dimethyl sulfoxide-d6 (DMSO-d6) as solvent. The chemical shifts of the carbons in the compounds were investigated using ^{13}C-NMR (APT) spectroscopy. By referencing the solvent peak, the chemical shifts of the carbons in the compounds were examined in positive and negative fields. In compounds a and b, the carbon chemical shifts are observed in similar regions. The carbons in the benzene ring and the methoxy group in compounds a and b exhibit chemical shifts in the positive field, while the other carbons in the structure show chemical shifts in the negative field. In compound c, the carbon chemical shifts are observed in the opposite field compared to compounds a and b. The chemical shifts of the carbons in the benzene ring and the methoxy group are observed in the negative field, while the other carbons show chemical shifts in the positive field.

Liquid chromatography-tandem mass spectrometry analysis

The LC/MS (Electrospray Ionisation-ESI) molecular ion peaks for compounds a, b, and c were identified at 265.99 $[M-H]^-$, 266.94 $[M-H]^-$, and 266.93 $[M-H]^-$ respectively, confirming the structures of these compounds. The physical properties of the synthesized compounds include white solids or powders, and they were obtained with high yields. In the mass spectrometry of compound (a), looking at the separated molecular ion peaks, the fragments of 72.99 [CHN_2S^{3-}] and 131.97 [$C_2H_2N_3S^{2\bullet}$] have been released, and the remaining compound has a peak at 135.04 g/mol [$C_8H_7O^{2\bullet}$]. In compound (b), the fragments of 58.98 [$CHNS^{2-}$] and 131.96 [$C_3H_2NOSO_2^{5-}$] are released, and the remaining ion peak is at 107.13 [$C_7H_7O^{3-}$]. Compound (c)'s mass spectrometry has detected no specific fragmentation product similar to the other compounds. In compound (c), the absence of fragmentation in the molecular ion peaks may be due to the methoxy functional group being attached to the phenyl ring in the para position and positioned away from the branched groups with electron density.

Thermal Analysis

Thermal analysis curves recorded because of thermal decomposition carried out in an inert nitrogen atmosphere in the range of 25-1000 °C are shown in Figures 3 and 4 for three samples combined. The decomposition steps of the samples whose weight loss curves are given in Figure 3 were determined to be close to each other. It was observed that the decomposition of the (a) molecule created better observable decomposition steps compared to other samples. The molecule with the most difficult decomposition steps to follow is the (c) derivative molecule, and this can be thought to be due to the methoxy functional group attached to the phenyl ring being attached in the para position and positioned away from the branched groups with electron density. Again, this may be the reason why the stability of the para derivative molecule is higher than the others. In all samples, it is seen that the first decomposition step starts at approximately 140 °C and ends at 200 °C. In this temperature range, the decomposition of the methoxy group attached to the phenyl ring is considered (experimental weight loss: 10.50%, theoretical weight loss: 11.61%). The next decomposition step is observed to start around 230 °C and end at 400 °C. The highest weight loss is observed in this temperature range, which can be interpreted as the decomposition of the thiazole group attached to the phenyl ring with the carbonyl bridge (experimental weight loss: 48.80%, theoretical weight loss: 49.45%). The temperature range that draws attention as the last decomposition step starts at 400 °C and ends in the 780 °C temperature regions. In this temperature range, the decomposition of the remaining phenyl and carbonyl groups of the organic molecule was observed (experimental weight loss: 38.20%, theoretical weight loss: 38.95%). As a result of thermal analysis, it was observed that approximately 1-2% black residues were present in the reaction vessel. Since the structure is completely organic, no residue was expected because of thermal analysis, but the 1-2% residue detected was interpreted as non-burnable carbonized carbon residue because of thermal decomposition carried out in an inert nitrogen atmosphere. It was confirmed by the differential thermal analysis (DTA) curves (Figure 4) that all thermal decomposition steps occurred under endothermic decomposition.

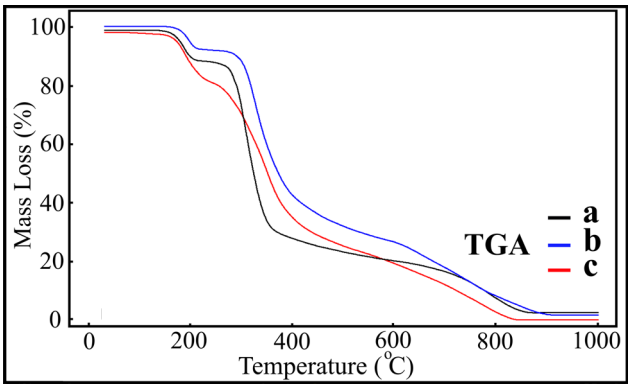

Figure 3. Thermal weight loss curves of o-, m-, p-methoxybenzamide derivative molecules

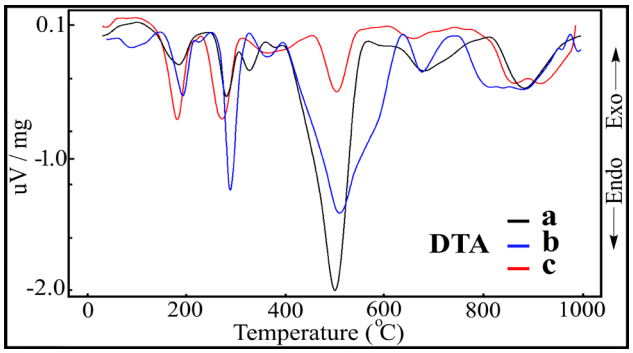

Figure 4. Differential thermal analysis curves of o-, m-, p-methoxybenzamide derivative molecules

CONCLUSION

The compounds N-(5-mercapto-1,3,4-thiadiazol-2-yl)-2-methoxybenzamide (a), N-(5-mercapto-1,3,4-thiadiazol-2-yl)-3-methoxybenzamide (b), and N-(5-mercapto-1,3,4-thiadiazol-2-yl)-4-methoxybenzamide (c) were obtained by the reaction of 5-amino-1,3,4-thiadiazole-2-thiol with 2-methoxybenzoyl chloride (a), 3-methoxybenzoyl chloride (b), and 4-methoxybenzoyl chloride (c), forming an amide bond. The antimicrobial properties of the obtained compounds and their potential as essential drug components in the medical field are attributed to the nature of the amide bond. Furthermore, heterocyclic compounds containing a 1,3,4-thiadiazole structure are essential due to their broad application fields. As a result of this study, methoxybenzamide derivatives containing 1,3,4-thiadiazole and amide bonds were obtained. The structural characterization of the obtained compounds was carried out using FTIR, MS-ESI, 1H NMR, 13C NMR APT spectroscopy, and elemental analysis. Thermal analysis (TGA/DTA/DrTG) examined their thermal stability. In conclusion, new compounds have been introduced to the chemical literature.

References

1. Prabukanthan P, Raveendiran C, Harichandran G, Seenuvasakumaran P. Synthesis, crystal growth, crystal structure, optical, thermal, biological and NLO studies of heterocyclic compound N-(1, 3-benzothiazol-2-yl)-2-methoxybenzamide. Results Chem. 2020;2:100083. doi:10.1016/j.rechem.2020.100083.
2. Wang L, Wang DH, Zhang GH, Xu D, Deng WX. Crystal structure, spectroscopic investigation and thermal properties of L-lysine p-toluenesulfonate. J Mol Struct. 2016;1108:179-186. doi:10.1016/j.molstruc.2015.11.019.
3. Mermer A, Bayrak H, Alyar S, Alagumuthu M. Synthesis, DFT calculations, biological investigation, molecular docking studies of β-lactam derivatives. J Mol Struct. 2020;1208:127891. doi:10.1016/j.molstruc.2020.127891.
4. John JS, Sajan D, Prabukanthan P, Philip R, Joy N. Enhanced NLO activity of organic 2-methyl-5-nitroaniline crystal: Experimental and computational investigation with and without silver addition. Opt Laser Technol. 2019;113:416-427. doi:10.1016/j.optlastec.2019.01.014.
5. Shkir M, Abbas H. Physico-chemical properties of L-asparagine L-tartaric acid single crystals: A new nonlinear optical material. Spectrochim Acta Part A Mol Biomol Spectrosc. 2014;118:172-176. doi:10.1016/j.saa.2013.08.086.
6. Prabukanthan P, Lakshmi R, Harichandran G, Sudarsana Kumar C. Synthesis, structural, optical and thermal properties of N-methyl N-aryl benzamide organic single crystals grown by a slow evaporation technique. J Mol Struct. 2018;1156:62-73. doi:10.1016/j.molstruc.2017.11.075.
7. Faizi MSH, Osório FAP, Valverde C. Synthesis, crystal structure, spectroscopic and nonlinear optical properties of organic salt: a combined experimental and theoretical study. J Mol Struct. 2020;1210:128039. doi:10.1016/j.molstruc.2020.128039.
8. Liu J, Zhou H, Lian Y, Feng Y, Fan T, Xu J, Xu X. Electrically controlled growths of 4-N,N-dimethylamino-40-N0 -methyl-stilbazolium tosylate (DAST) organic microcrystals. Appl Phys A. 2020;126(3). doi:10.1007/s00339-020-3424-9.
9. Liu H, Li M, Wang P, Hu Z, Yin H. Numerical simulation of the flow and mass transport during the growth of ADP crystals by additional stirrer. J Cryst Growth. 2020;534:125507. doi:10.1016/j.jcrysgro.2020.125507.
10. Ningaiah S, Bhadraiah UK, Sobha A, Shridevi D. Synthesis of novel pyrazolyl-1,3,4-thiadiazole analogues. Polycyclic Aromatic Compounds. 2020;42(4):1249-1259. doi:10.1080/10406638.2020.1773875.
11. Li M, Zhao B. Progress of the synthesis of condensed pyrazole derivatives (from 2010 to mid-2013). Eur J Med Chem. 2014;85:311-340.
12. Radwan A, Khalid M, Amer H, Alotaibi M. Anticancer and molecular docking studies of some new pyrazole-1-carbothioamide nucleosides. Biointerface Res Appl Chem. 2019;9:4642-4648.
13. Ehab M, Gedawy AE, Kassab AM, El K. Design, synthesis and biological evaluation of novel pyrazole sulfonamide derivatives as dual COX-2/5-LOX inhibitors. Eur J Med Chem. 2020;189:112066.
14. Vijesh AM, Isloor AM, Shetty P, Sundershan S, Fun HK. New pyrazole derivatives containing 1,2,4-triazoles and benzoxazoles as potent antimicrobial and analgesic agents. Eur J Med Chem. 2013;62:410-415.
15. Neidiane R, Trindade PR, Lopes LM, Naves JO, Fajemiroye PH, Alves NO, Amaral LM, Liao ACS, Rebelo CH, Castro VA, et al. The newly synthesized pyrazole derivative 5-(1-(3-fluorophenyl)-1H-pyrazol-4-yl)-2H-tetrazole reduces blood pressure of spontaneously hypertensive rats via NO/cGMO pathway. Front Physiol. 2018;9:1073-1083.
16. Malvar DC, Ferreira RT, de Castro RA, de Castro LL, Freitas AC, Costa EA, Florentino IF, Mafra JC, de Souza GE, Vanderlinde FA. Antinociceptive, anti-inflammatory and antipyretic effects of 1.5-diphenyl-1H-pyrazole-3-carbohydrazide, a new heterocyclic pyrazole derivative. Life Sci. 2014;95(2):81-88.
17. Reddy GM, Jarem RG, Grigory VZ, Gundala S, Reddy NB. Pyranopyrazoles as efficient antimicrobial agents: Green, one pot and multicomponent approach. Bioorg Chem. 2019;82:324-331.
18. Silva VLM, Elguero J, Silva AMS. Current progress on antioxidants incorporating the pyrazole core. Eur J Med Chem. 2018;156:394-429.
19. Ansari A, Ali A, Asif M, Shamsuzzaman S. Biologically active pyrazole derivatives. New J Chem. 2017;41(1):16-41.
20. Satish G, Srinivasa RA, Jeevan LP, Rajeswar RV, Santhosh P. An efficient synthesis of pyrazolyl-1,2,3-thiadiazoles via Hurd–Mori reaction. J Heterocycl Chem. 2019;56:2163-2169.
21. Serban G, Stanasel O, Serban E, Bota S. 2-Amino-1,3,4-thiadiazole as a potential scaffold for promising antimicrobial agents. Drug Des Devel Ther. 2018;12:1545-1566.
22. Serban G. Synthetic compounds with 2-amino-1,3,4-thiadiazole moiety against viral infections. Molecules. 2020;25(4):942-964.
23. Farghaly TA, Abdallah MA, Masaret GS, Muhammad ZA. New and efficient approach for synthesis of novel bioactive [1,3,4] thiadiazoles incorporated with 1,3-thiazole moiety. Eur J Med Chem. 2015;97:320-333.
24. Chidananda N, Poojary B, Sumangala V, Kumari NS, Shetty P, Arulmoli T. Facile synthesis, characterization and pharmacological activities of 3,6-disubstituted 1,2,4-triazolo[3,4-b][1,3,4]thiadiazoles and 5,6-dihydro-3,6-disubstituted-1,2,4-triazolo[3,4-b][1,3,4]thiadiazoles. Eur J Med

Chem. 2012;51:124-136.
25. Oruc EE, Rollas S, Kandemirli F, Shvets N, Dimoglo AS. 1,3,4-thiadiazole derivatives. Synthesis, structure elucidation, and structure-antituberculosis activity relationship investigation. J Med Chem. 2004;47(27):6760-6767.
26. Megally ANY, Kamel MM. Synthesis and anticancer evaluation of 1,3,4-oxadiazoles, 1,3,4-thiadiazoles, 1,2,4-triazoles and Mannich bases. Chem Pharm Bull. 2015;63(5):369-376.
27. Dawood KM, Farghaly TA. Thiadiazole inhibitors: A patent review. Expert Opin Ther Patents. 2017;27:477-505. Serban G. Future prospects in the treatment of parasitic diseases: 2-amino-1,3,4-thiadiazoles in leishmaniasis. Molecules. 2019;24:1557.
28. Brunton L, Chabner B, Knollman BG. Goodman & Gilman's the pharmacological basis of therapeutics. New York: McGraw-Hill; 2010.
29. Pattabiraman VR, Bode JW. Rethinking amide bond synthesis. Nature. 2011;480:471-479.
30. Kaspar AA, Reichert JM. Drug future directions for peptide therapeutics development. Discov Today. 2013;18:807-817.
31. Brown DG, Bostrom J. Analysis of past and present synthetic methodologies on medicinal chemistry: Where have all the new reactions gone? J Med Chem. 2016;59:4443-4458.
32. Ragavan RV, Vijayakumar V, Suchetha Kumari N. Synthesis and antimicrobial activities of novel 1,5-diaryl pyrazoles. Eur J Med Chem. 2010;45(3):1173-1180.
33. Ines V, Andrea PR, Kata MM, Karmen B, Branimir B. Synthesis and biological validation of novel pyrazole derivatives with anticancer activity guided by 3D-QSAR analysis. Bioorg Med Chem. 2012;20:2101-2110.
34. Rai NP, Narayanaswamy VK, Shashikanth S, Arunachalam PN. Synthesis, characterization and antibacterial activity of 2-[1-(5-chloro-2-methoxy-phenyl)-5-methyl-1H-pyrazol-4-yl]-5-(substituted-phenyl)-[1,3,4]oxadiazoles. Eur J Med Chem. 2009;44(11):4522-4527.
35. Vijesh AM, Isloor AM, Shetty P, Sundershan S, Fun HK. New pyrazole derivatives containing 1,2,4-triazoles and benzoxazoles as potent antimicrobial and analgesic agents. Eur J Med Chem. 2013;62:410-415.
36. Bekhit AA, Ashour HMA, Ghany YSA, Bekhit AED, Baraka A. Synthesis and biological evaluation of some thiazolyl and thiadiazolyl derivatives of 1H-pyrazole as anti-inflammatory antimicrobial agents. Eur J Med Chem. 2008;43(3):456-463.
37. Kasımogulları R, Bülbül M, Arslan BS, Gökçe B. Synthesis, characterization and antiglaucoma activity of some novel pyrazole derivatives of 5-amino-1,3,4-thiadiazole-2-sulfonamide. Eur J Med Chem. 2010;45(11):4769-4773.
38. Perea S, Patterson TF. Clin Infect Dis. 2002;35:1073.
39. Chakrabarti A. Regional Health Forum. 2011;15:97.
40. Tscherner M, Schwarzmüller T, Kuchler K. Pharmaceuticals. 2011;4:169.
41. White MA, Marr KA, Bowden RA. Clin Microbiol Rev. 1998;11:382.
42. Ghannoum MA, Rice LB. Clin Microbiol Rev. 1999;12:501.
43. Matysiak J, Niewiadomy A, Krajewska-Kułak E, Ma˛cik-Niewiadomy G. Il Farmaco. 2003;58:455.
44. Malik MA, Al-Thabaiti SA, Malik MA. Int J Mol Sci. 2012;13:10880.
45. Altıntop MD, Özdemir A, Turan-Zitouni G, Ilgın S, Atlı Ö, Iscan G, Kaplancıklı ZA. Eur J Med Chem. 2012;58:299.
46. Tyrkov AG, Abdel'rakhim MA, Sukhenko LT, Degtyarev OV. Pharm Chem J. 2014;47:589.
47. Altıntop MD, Kaplancıklı ZA, Çiftçi GA, Demirel R. Eur J Med Chem. 2014;74:264.
48. Vembu S, Pazhamalai S, Gopalakrishnan M. Med Chem Res. 2016. Available from: http://dx.doi.org/10.1007/s00044-016-1627-6.
49. Kategaonkar AH, Pokalwar RU, Sonar SS, Gawali VU, Shingate BB, Shingare MS. Eur J Med Chem. 2010;45:1128.
50. Kategaonkar AH, Labade VB, Shinde PV, Kategaonkar AH, Shingate BB, Shingare MS. Monatsh Chem. 2010;141:787.
51. Shashikumar ND, Krishnamurthy G, Bhojyanaik HS, Lokesh MR, Jithendrakumara KS. J Chem Sci. 2014;126:205.
52. Łukowska-Chojnacka E, Mierzejewska J, Milner-Krawczyk M, Bondaryk M, Staniszewska M. Synthesis of novel tetrazole derivatives and evaluation of their antifungal activity. Bioorg Med Chem. 2016;24:6058-6065. doi:10.1016/j.bmc.2016.09.066.
53. Çolak N, Şahin F, Erten G, Muhammet SM. Synthesis, Structural Analysis, Antimicrobial Activity and The Molecular Electrostatic Potential Surface (MEP) of 2/3/4-Chloro BenzamideSpiro[Benzo[B]Thiophene-Dioxolane] Derivatives. Süleyman Demirel University Faculty of Arts and Sciences Journal of Science. 2024;19(1):53-62.
54. Serdaroğlu G, Uludag N, Colak N, Rajkumar P. Nitrobenzamido substitution on thiophene-3-carboxylate: Electrochemical investigation, antioxidant activity, molecular docking, DFT calculations. J Mol Struct. 2023;1271:134030.

Supplementary Materials

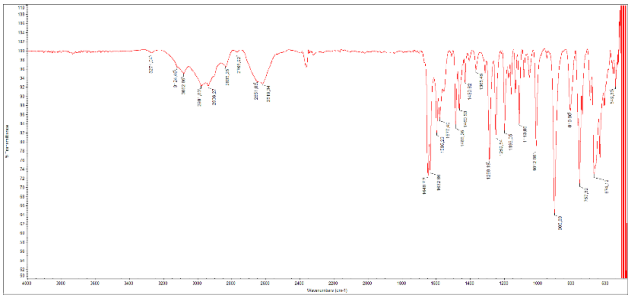

Fig S1. FTIR spectrum of (**a)** compound

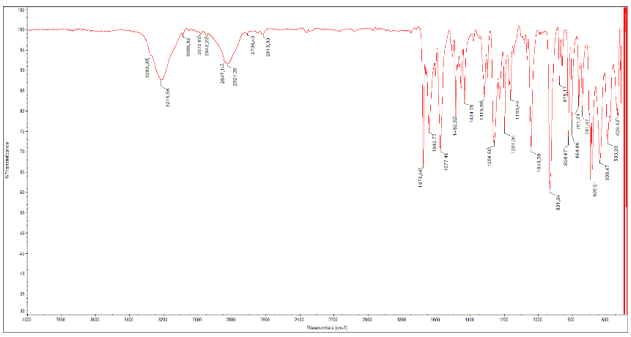

Fig S2. FTIR spectrum of (**b)** compound

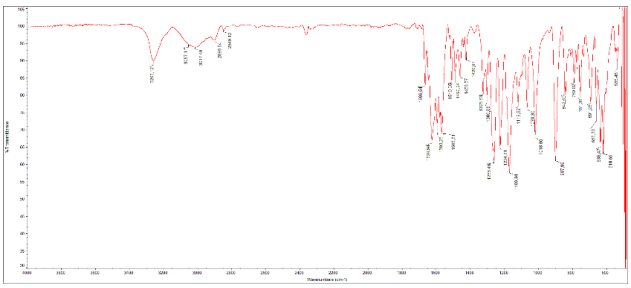

Fig S3. FTIR spectrum of (**c**) compound

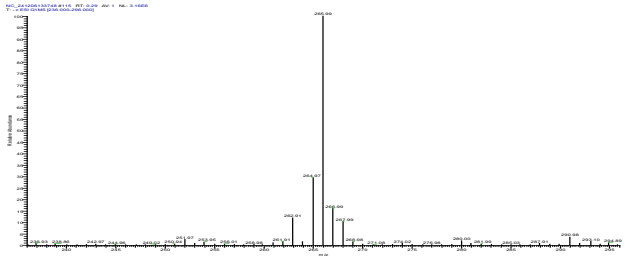

Fig S4. LS/MS (-ESI) spectrum of (**a**) compound

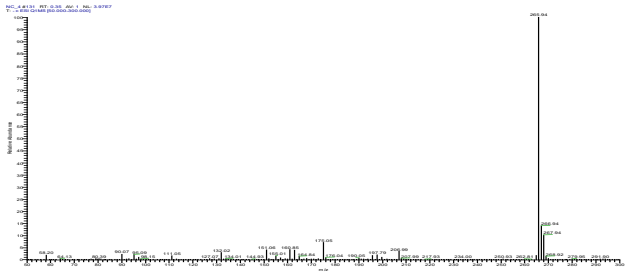

Fig S5. LS/MS (-ESI) spectrum of (**b**) compound

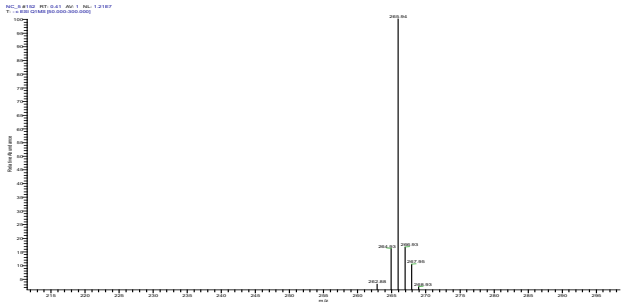

Fig S6. LS/MS (-ESI) spectrum of (**c**) compound

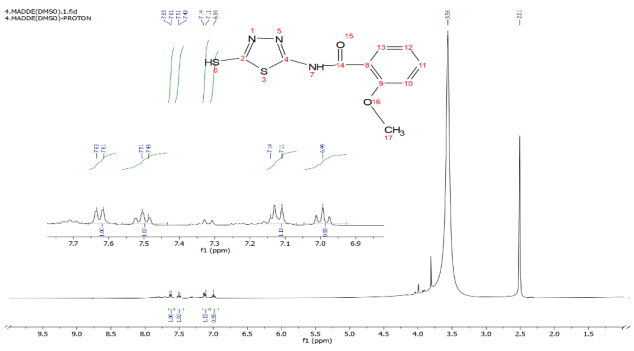

Fig S7. ^{1}H-NMR spectrum of (**a**) compound

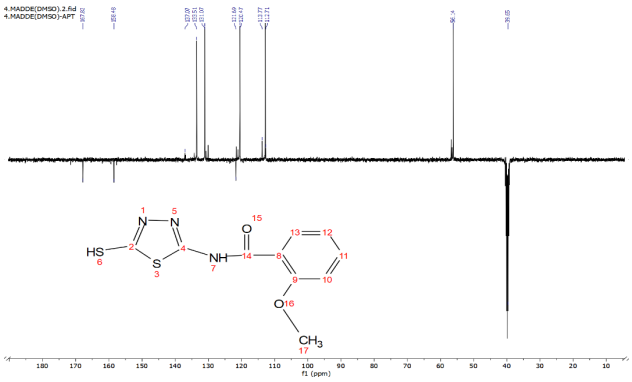

Fig S8. ^{13}C-NMR APT spectrum of (**a**) compound

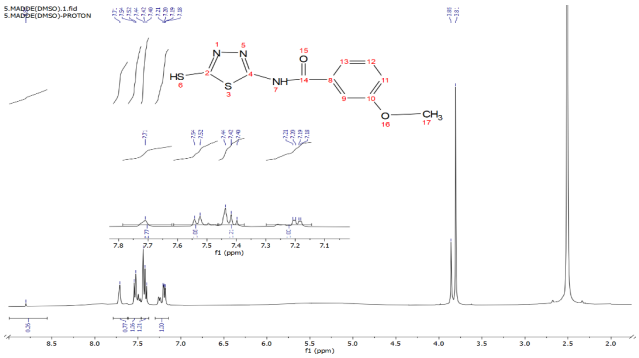

Fig S9. ^{1}H-NMR spectrum of (**b**) compound

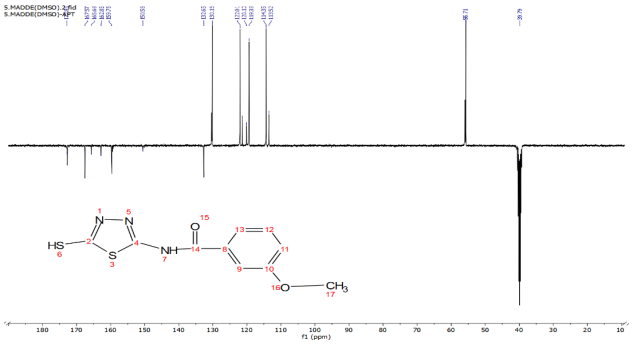

Fig S10. ^{13}C-NMR APT spectrum of (**b**) compound

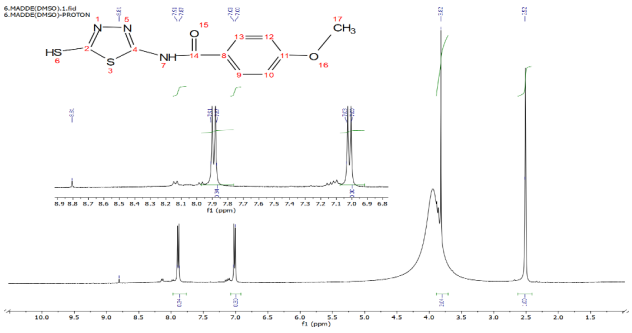

Fig S11. ^{1}H-NMR spectrum of (**c**) compound

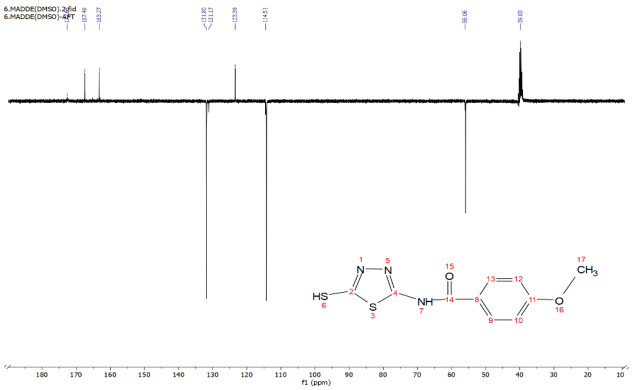

Fig S12. ^{13}C-NMR APT spectrum of (**c**) compound